ALPHA FOUNDATION FOR THE IMPROVEMENT OF MINE SAFETY AND HEALTH

Final Technical Report

Project Title: Minimizing Rib Failure Hazards – Feasibility Demonstration for Low-Cost, High-Resolution Rib Monitoring - Objective 3

Grant Number: AFCRFP20 - 111

Organizations: Colorado School of Mines
1500 Illinois St.
Golden, CO 80401

West Virginia University
886 Chestnut Ridge Road, PO Box 6845
Morgantown, WV 26506-6845

Principal Investigators: Drs. I. Tulu (WVU) and G. Walton (CSM)

Period of Performance: January 1, 2021 – June 30, 2023

1.0 Executive Summary:

Problem statement: In U.S. coal mines, rib falls are the one of the leading causes of ground-fall fatalities, and the fraction of "falls of rib or face" has increased recently (MSHA, 2019; Mohamed et al., 2020). The development of a rib hazard depends on factors like rib geology, rib height, overburden stress and mining-induced stresses. It is possible to respond to an emerging potentially hazardous condition to prevent accidents, if the potentially hazardous condition is identified. Therefore, proper inspection to characterize rib geology and to identify deteriorating ground conditions and rapid response to prevent further deterioration can protect miners from possible fall of ground accidents. However, often it is neither practical nor economical to inspect vast areas of mine workings with limited personnel. This inspection can be automated using the current mobile low-cost LIDAR systems that can be mounted on a vehicle or carried by a miner. However, it is required to perform a scientific, practical and regulatory assessment of the potential for implementation of low-cost vehicle-mounted laser scanning for rib monitoring and characterization.

Research approach: Safety in underground coal mines would be improved by adapting mobile low-cost LIDAR systems to underground coal mining industry for rib monitoring and characterization. This project performed an assessment of a low-cost hand-held and/or vehicle-mounted laser scanner and commercial Simultaneous Localization and Mapping (SLAM) software for rib inspection. The research accomplished in this project includes: (i) A critical review of a LIDAR system that represents the existing technologies was conducted to determine what is necessary to make that system compliant with the requirements for use in a potentially explosive atmosphere. (ii) Data were collected in a controlled laboratory setting and an experimental underground coal mine, and these data were used to evaluate potential reliability in the context of rib geology characterization and convergence detection.

Accomplishments: An overview of the Mine Safety and Health (MSHA) approval process and tests and inspections that might be conducted by MSHA for products such as the GeoSLAM Zeb Horizon portable LiDAR scanner was provided. Recommendations were provided for those who wish to design and manufacture a portable LiDAR system for use in gassy underground mines in the United States. This research provides guidelines and roadmap for developing and getting approval for a permissible mobile LiDAR system. We also provide an assessment of the potential for such systems to be used for (i) monitoring rib deformation, movement, or changes and (ii) estimation of coal rib lithology from point cloud data.

Expected impact on mining health and safety: The report and methods detailed during this research are immediately available to the mining industry, Mine Safety and Health Administration (MSHA) and National Institute for Occupational Safety and Health (NIOSH) to consider for development of a mobile LiDAR system that can be used in underground coal mining environment. The research presented in this report has found that the mobile LiDAR measurements can detect rock falls from ribs or roofs that are 6 cm or greater in size. However, detecting small physical changes on the rib (< 6cm) proved difficult for the mobile LiDAR unit used in this study but was detectable by a static LIDAR. This study also demonstrated the possibility of differentiating different coal rib lithologies based on the LIDAR intensity measurements. Currently, there are no permissible portable LIDAR devices. This report also summarizes the several technical and administrative challenges for developing a permissible (intrinsically safe) LIDAR unit.

2.0 Problem Statement and Objective:

Research Focus Area

The goal of this research is to perform the required scientific, practical and regulatory assessment of the potential for implementation of low-cost vehicle-mounted laser scanning for rib monitoring and characterization in underground coal mining sector to reduce the exposure of coal mine workers to rib falls. This project focused on the underground coal mining industry and addresses the Alpha Foundation Research Topical Area "*Health and Safety Interventions*" with a specific emphasis on "*prevention of unstable ground conditions that result in collapses and roof/rib falls*." This work is directly relevant to Alpha Foundation Priority *Area "Ground Control - Prevention of unstable ground conditions that result in collapses; roof and rib falls; and injuries due to insufficient support coverage.*"

Problem Statement

In 2019, underground mining accounted for about 38% of all coal production in the United States (MSHA, 2020). Mohamed et al. (2020) stated that over the past decade, falls of rib or face have accounted more than 50% of the ground-fall fatalities in U.S. coal mines, and more recently, this proportion had increased to 80%. To address the fatalities and injuries from falls of rib, NIOSH researchers developed a design methodology for rib control in U.S. coal mines, the Coal Pillar Rib Rating (CPRR).

The CPRR quantifies the quality of coal ribs and considers the variation on visual factors like seam lithology and rib height Mohamed et al. (2020). In addition, CPRR method recognizes that rib condition mapping and monitoring are an integral part of the rib hazard identification (Guner et al., 2023; Mohamed et al., 2020). Therefore, miners can be protected from potential fall of rib accidents with adequate inspection to characterize rib geology, identify worsening ground conditions, and prompt intervention to prevent further deterioration. However, in many cases it is neither practicable nor cost-effective to inspect substantial portions of mine workings. Adapting mobile low-cost LIDAR systems to underground coal mining industry for rib monitoring and characterization would solve this problem and can improve the safety of the coal miners. To allow for the use of such systems, practical and regulatory assessment of this new technology for implementation in the underground coal sector is necessary, as are assessments of current technical capabilities and potential challenges in application.

Background

Rib falls are the leading cause of ground-fall fatalities in U.S. coal mines, and the proportion of ground-fall fatalities corresponding to "falls of rib or face" has increased in recent years (MSHA, 2019; Mohamed et al., 2020). In U.S. underground coal mines, rib supports are designed by trial and error (NIOSH, 2023). NIOSH recently developed the CPRR method that quantifies the quality of coal ribs (Mohamed et al., 2020), which was originally based on a combination of numerical model results and empirical observations. The previously developed Analysis and Design of Rib Support (ADRS) system (Colwell & Mark, 2005) was a precursor to the design approach associated with the CPRR, but tended to simplify the geological factors that affect stability and was specific to Australian coal mines.

The CPRR system assigns a rating corresponding to a pillar rib's inherent ability to resist instability based on rib geological characteristics and geometry. This rating can then be combined with a measure of the degree of loading expected on the rib (Mohamed et al., 2020 use depth to entry) to establish a rib stability rating (Mohamed et al., 2020 use rib factor of safety, or "RibFOS"). Using the RibFOS value as an

indicator of unsupported rib stability, Mohamed et al. (2020) illustrate how rib performance relates to support density and RibFOS in the context of several case studies.

Guner et al. (2023) summarizes the various factors that have been identified to influence rib performance and support design in the US and Australia (Figure 1). From these factors, rib height, rib lithology/geology, support density and roof/floor/rib conditions can be gathered by visual inspections from field surveys and mapping. In situ and induced stresses can be estimated using numerical or analytical models, and strength parameters can be measured in the lab or on the field. Visual inspection and monitoring are an integral part of the rib stability assessment. Heasley and Chekan (1998), Karabin and Evanto (1999) and Lawsoon et al. (2012) combined stress analysis and visual observations to assess the stability of the ribs. CPRR and ADRA were developed from the back analysis of the data gathered from underground mines with filed monitoring, rib conditions, and analytical/numerical analysis. Therefore, rib inspection, monitoring and condition mapping are necessary for successful rib support design and hazard detection.

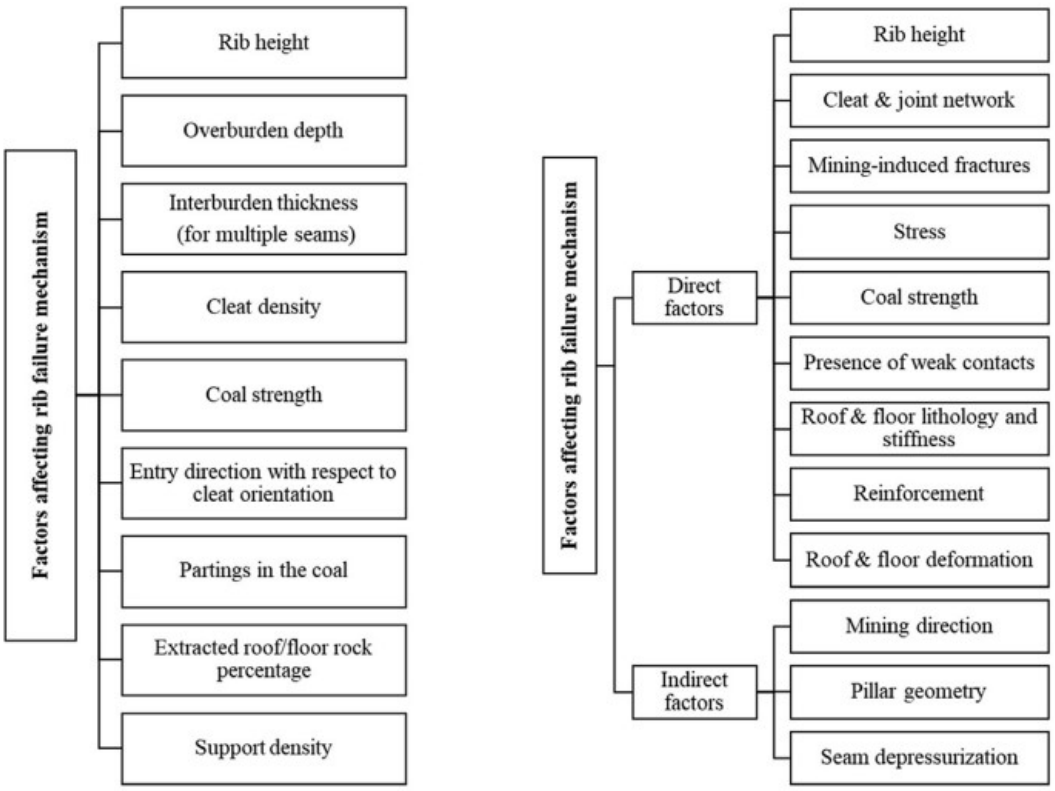

Figure 2.1. *Factors affecting the rib performance (Guner et al., 2023).*

Mapping in an underground coal mine is essential for stability assessment (Heasley et al., 2018; Klemetti et al., 2020; Van Dyke et al., 2020) as well as Coal Pillar Rib Rating determination and rib-hazard detection (Mohamed et al., 2020). The utilization of stability mapping with current sensor technologies like LIDAR and Photogrammetry in US underground coal mines has been limited (or not applicable) mainly due to intrinsic safety requirements (Slaker and Mohamed, 2017). In addition, in underground mines, efficient and quick mapping of mine entries with LIDAR and camera technologies with simultaneous localization has been challenging due to unavailability of Global Position System (GPS) data. Recent advances in sensor technology and simultaneous localization and mapping (SLAM)

algorithms, however, have led to the development of portable and mobile laser scanning devices that can be used in GPS-denied environments.

Unlike metal/nonmetal underground mines, application of new technologies to underground coal mining requires special consideration of regulatory and environment-specific challenges. Before electric equipment can be used in gassy mines in the U.S., they must first have been approved for such use by MSHA. The Federal Mine Safety and Health Act of 1977 (30 U.S.C. 801) (Mine Act) requires the Mine Safety and Health Administration (MSHA) to establish requirements for the technical design, construction, and testing of electrical products that must be approved by MSHA prior to use in gassy mines. MSHA's approval process includes testing and evaluation of the products, either by MSHA or by an independent laboratory.

Specific Research Objective and Tasks

Colorado School of Mines (CSM) and West Virginia University (WVU) Mining Engineering researchers performed a two-year study to perform practical and regulatory assessment of a single, representative, LIDAR system that is being investigated for use in underground coal mine to determine: (i) what is necessary to make that system compliant with the requirements for use in a potentially explosive atmosphere and (ii) if this or similar LiDAR systems with SLAM technology can be used for rib inspection, monitoring, characterization, and condition mapping. The following specific research objective and research tasks were undertaken:

Research Objective: Establish Feasibility of Low-Cost Mobile LiDAR as a Practical Rib Monitoring Technology

- *Research Task 1:* Evaluate potential for MSHA approval of available low-cost LIDAR technology.
- *Research Task 2:* Collect in-mine data with low-cost LiDAR.
- *Research Task 3:* Evaluate accuracy of SLAM-based rib deformation monitoring.
- *Research Task 4:* Evaluate potential for estimation of rib lithology from point cloud data.

3.0 Research Approach:

This study's goal is to carry out the necessary technical, practical, and regulatory evaluation of the potential for implementing low-cost vehicle-mounted laser scanning for rib monitoring and characterization in underground coal mining to reduce the risk of injuries and fatalities due to rib falls. The following describes the objective and tasks that were undertaken to achieve this research goal.

<u>Research Objective:</u> Establish Feasibility of Low-Cost Mobile LiDAR as a Practical Rib Monitoring Technology.

In this section of the report, we describe the research performed to evaluate practical and regulatory considerations related to application of a commercial LiDAR system and accompanying SLAM software, Zeb Horizon of GeoSLAM (Figure 3.1), which we consider as representative technology for adapting this or similar mobile low-cost LiDAR systems to underground coal mining industry for rib monitoring and characterization.

Figure 3.1. *GeoSLAM ZEB Horizon.*

Zeb Horizon has a maximum range of 100 meters, can scan at a rate of 300,000 points per second using 16 sensors simultaneously, and can run continuously for about 3 hours on a single battery charge (GEOSLAM, 2020). The LiDAR weighs just 1.49 kg, designed to be carried by a person, and a data logger that fits in a backpack must be attached to the scanner through wires. In an underground mine, where the surroundings are typically dark, muddy, or wet, this design makes it easier to carry the equipment. It can also be attached on a car, a drone, or any moving vehicles.

Figure 3.2. *GeoSLAM ZEB Horizon attached to car and drone (Optron, 2023).*

***Research Task 1:* Evaluate potential for MSHA approval of available low-cost LIDAR technology.**

This task was performed by Kevin Hedrick as an independent consultant. In this task, an overview of the Mine Safety and Health (MSHA) approval process and tests and inspections that might be conducted by MSHA for products such as the GeoSLAM Zeb Horizon portable LiDAR scanner was provided. Potential problem areas are identified with the information at hand; foremost among those are spark-ignition hazards associated with the battery pack and sensor motor. Another significant concern is the potential motivation of the manufacturer to expend the resources necessary to redesign the product to meet MSHA's requirements. Also, the ability of a single entity to fully document and control the design of the product can be problematic, as components such as the sensor and memory sticks are purchased, and the manufacturer may not wish to share the design documentation. It is noteworthy that there are no known issues with the basic technologies used with this type of equipment.

Recommendations are provided for designers when developing a new portable LiDAR unit. The designers should consult MSHA's requirements, and, if necessary, utilize outside experts in the field of intrinsic safety. MSHA approves the design of this type of equipment, so it is important to develop the proper documentation to both satisfy MSHA's requirements and allow for manufacturing flexibility.

***Research Task 2:* Collect in-mine data with low-cost LiDAR.**

Rib and roof fall incidents in mining typically result from hazards that develop over time. Geology, excavation geometry, overburden stress, and mining-induced stresses are some of the factors that affect how hazards occur. Hazard mapping and monitoring in an underground mine is essential for roof and rib stability assessment. GeoSLAM ZEB-Horizon, a SLAM-based laser scanning system, allows for easy and quick mapping of underground coal pillar ribs. SLAM is the computational approach for mapping of an environment while simultaneously keeping track of the location of active-remote-sensing-system within the environment (Ravel et al., 2019). Mapping with the ZEB-Horizon produces point-clouds, which are essentially sets of three-dimensional point coordinates (X, Y, Z) and point attributes. One of those attributes is the intensity values, which is a measure of the laser energy that returns to the scanner after reflecting off a material. Intensity values are related to the color of a surface, so if it's darker, associated intensity values tend to be closer to zero, while lighter surfaces tend to be associated with higher return intensities. We used underground experiments to evaluate the potential to monitor rib deformations, characterize rib geology, and assess entry rib conditions from the point cloud data. Due to the permissibility requirements, in-mine tests were performed in the experimental coal mine of the Pittsburgh Mining Research Division (PMRD) of NIOSH.

Experiment #1: Detection of changes on the floor with the ZEB Horizon

This experiment took place in the experimental research mine at PMRD of NIOSH at Bruceton Pittsburgh, Pennsylvania. This experiment's goal is to evaluate the potential of identifying induced rockfalls using the LiDAR system with SLAM technology. The approaches used on this experiment are (i) artificially generating/inducing rock falls by placing different size rock pieces on the mine entry floor, (ii) assessing the minimum size of a rock that can be detected after applying the change detection algorithms by comparing different point clouds (before and after rock pieces were placed on the floor) generated by the ZEB Horizon from the same location. The following specific steps were followed in this experiment:

1. To map the initial entry and floor conditions, two surveys were conducted with traverses of one loop and two loops.
2. To represent rock falls from the rib, seven rock pieces of various sizes were chosen, and their dimensions (length and width) were roughly measured.
3. To artificially induce rock falls, rock pieces were placed on the floor. Figure 3.2 shows the induced rock falls, seven pieces, on the entry floor.
4. To map the final entry and floor conditions, three scans were performed with traverses of one loop, two loops, and three loops.

Figure 3.2. *Artificially induced rock falls, seven rock pieces, on the entry floor.*

Experiment #2: Detection of changes on the rib with the ZEB Horizon & I-Site 8200ER

The second experiment also took place in the PMRD experimental coal mine. The objective was to compare the potential of mobile and static LiDAR for monitoring rib deformation, movement, or changes. In this experiment, rock pieces from the coal pillar rib were artificially removed to induce changes on the rib. Before and after 3D point clouds were compared to evaluate the potential of rib monitoring. In this experiment, the mobile LiDAR system using SLAM was compared against a static LiDAR system (I-Site 8200).

Figure 3.3 shows the plan view of the 3D point clouds generated by Zeb Horizon (on the left) and I-Site 8200 (on the right). The experiment consisted of removing rock/coal pieces from the rib and conducting surveys both before and after the removal. Three surveys, where different numbers or loops (from 1 to 3) were traversed, were carried out using the mobile LiDAR. The number of points per unit area increases when traverses are completed with more loops during the survey, increasing the point density on the

surface of the rib. Only two scans were performed with the static LiDAR, before and after removing the rocks, and only one entry was mapped compared to all four entries around the pillar mapped by mobile LiDAR. The red circle on Figure 3.3 shows the rib where the changes were induced. Dr. Brent Slaker and Nicole Evanek from PMRD/NIOSH performed the I-Site 8200 survey and provided the raw point cloud data.

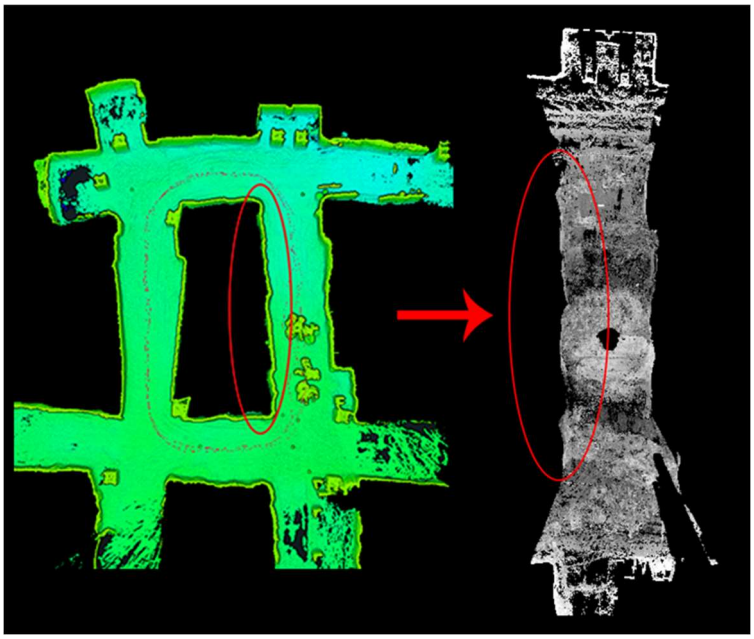

Figure 3.3. *Point clouds generated by Zeb Horizon (left) and I-Site 8200 (right).*

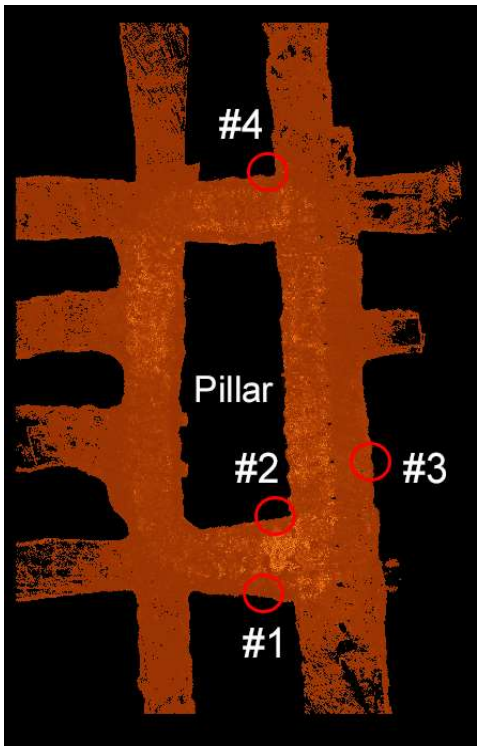

Figure 3.4. *Plan view of the point clouds map to identify lithological changes.*

Experiment #3: Identification of lithologies on coal pillar ribs

The third experiment was conducted in the experimental coal mine of PMRD, where coal rib lithology includes rock partings and shale bands and are also partially covered in shotcrete. This rib lithology and partial shotcrete coverage makes this an ideal place to evaluate the potential of identifying rib lithological differences from point clouds. The purpose of this experiment was to determine whether the point cloud data from mobile LiDAR could be used to detect the presence and locations of coal, rock partings and shotcrete in/on the rib. Figure 3.4 shows the pillar and the entries around it where surveys were performed. Red circles represent the locations where the lithological changes were assessed.

***Research Task 3:* Evaluate accuracy of SLAM-based rib deformation monitoring.**

The objective of the first experiment is to evaluate the potential of identifying the induced rockfalls using the LiDAR system with SLAM technology, and the second experiment is to compare mobile and static LiDARs potential of monitoring rib deformation, movement, or changes. Therefore, both experiments were performed to evaluate the accuracy of SLAM-based rib deformation monitoring.

LiDAR data gathered during these experiments were processed using a series of software and algorithms to compute and visualize the changes between different point clouds. During the LiDAR survey, commercial SLAM LiDAR software, a Continuous Time (CT) SLAM technology that was developed by GeoSLAM, was applied (GeoSLAM, 2021). Khan et al. (2021) summarized the steps followed during a LiDAR survey as: (i) SLAM software creates an initial map of its surroundings using the initial data that was collected from the LiDAR sensor. (ii) The starting point of the survey is set as the initial location of the LiDAR, then the software computes and extracts landmarks based on the generated map and the information of the environment before the equipment is mobilized. (iii) When the operator starts walking and mobilizes the LiDAR, mapping and localization processes are executed recursively. A new local map of the environment is generated, and new landmarks are identified and extracted by the software. (iv) SLAM software then associates the newly observed landmarks with the earlier ones and updated the position of the LiDAR. (v) As the operator moves and new information is gathered from LiDAR sensor, location of the LiDAR is continuously updated by the association of the new landmarks with the previous ones. It is recommended to traverse a loop to the starting point of the survey to improve the accuracy of the localization and local maps. It isn't in the scope of this research to evaluate the different SLAM algorithms, but it is important to indicate the GeoSLAM is one of the first and most widely used algorithms available in the industry.

After the survey was completed, the GeoSLAM Hub was used to process the raw Zeb Horizon data to convert LiDAR sensor data to a usable format. This software allows the user to export raw data in any common LiDAR survey file format. In our research, we used a LAZ file format since it can store all the information in a compressed file. Then LAZ file was imported into CloudCompare, an open-source 3D point cloud and triangular mesh processing software (CloudCompare, 2016). It was developed, as its name indicates, to compare two point clouds and became an independent open-source project. CouldCompare can visualize the large size of point clouds data efficiently, and there are different algorithms available to perform projections, registrations, distance computations, statistics computations, segmentation, geometric features estimations, etc.

In our research, we first performed a manual coarse point cloud alignment. Then we used the Iterative Closest Point (ICP) algorithm to automatically finely register and align two point clouds that were compared for identifying any changes. The ICP technique is frequently utilized for registering 3D LiDAR data (Rusinkiewicz & Levoy, 2001). The algorithm applies a simple nearest neighbor approach by iteratively associating every point from a base point cloud to the closest points from the second point cloud. Then, it uses data association to find the transformation matrix so that the point clouds are moved on top of each by minimizing the distances between the corresponding points from two point clouds. The algorithm iterates over the solution, repeating the data association and transformation many times, until it reaches the alignment with a predefined error metric (the default value of 0.01 mm was used in our analysis). Figure 3.5 visualizes this alignment of two different LiDAR survey data from the second experiment using the ICP algorithm.

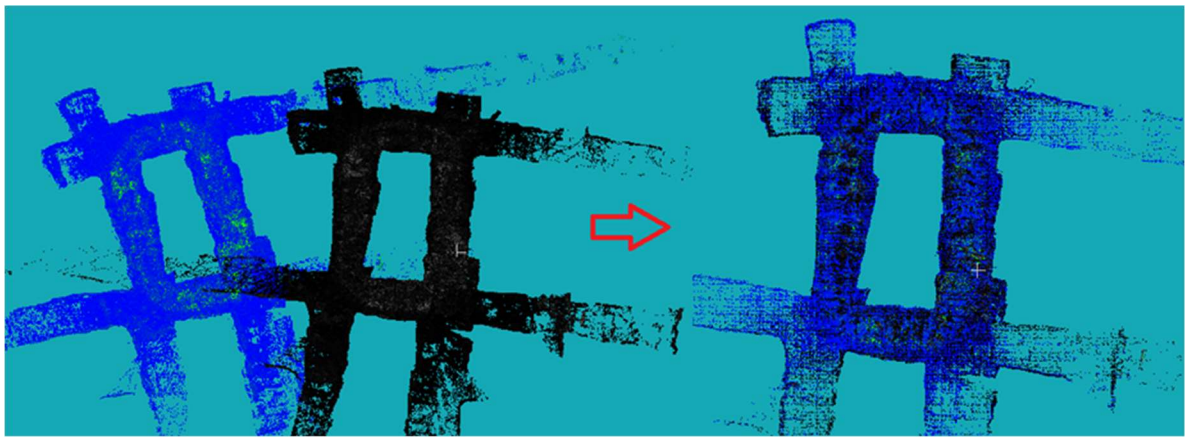

Figure 3.5. *Eperiment#2 point clouds' original positions and after being translated/rotated.*

The next step in our approach is to apply the Multiscale Model-to-Model Cloud Comparison (M3C2) algorithm to detect any difference between two point clouds aligned by the application of the ICP. M3C2 algorithm compares two point clouds: One of them is labeled as reference and other one as aligned. The algorithm can use the whole point cloud, or a subsample of that cloud during the computation and the subsample option is provided to reduce the computation time of processing of the large data sets. M3C2 calculates a local average cloud-to-cloud distance for a point in the reference cloud using a search cylinder projected along a locally oriented normal vector. The distance calculated is assigned then as an attribute of the point (Lague et al., 2013).

<u>Research Task 4:</u> Evaluate potential for estimation of rib lithology from point cloud data.

In this task, it was demonstrated that SLAM-based LiDAR can be used to recognize the changes in the lithology from the intensity values. First, in a laboratory setup, LiDAR scans of rock cores of different lithologies were collected to investigate the relationship between the lithology, the intensity values and the measurement distance. The LiDAR data was processed with Cloud Compare, and One-Way ANOVA was used to compare the intensity values obtained for each lithology. Then to verify that the intensity values can be used to estimate the lithology of a coal rib on the field too, the third field experiment (see research task 2) data was analyzed.

Laboratory experiments were performed in the Triaxial Laboratory in the Benjamin M. Statler College of Engineering and Mineral Resources building. This laboratory was chosen because it includes a large table

in the middle with enough space to place for the rock sample and LiDAR system to be placed at different distances up to 150cm. During the experiments, the distance between the LiDAR and rock samples were changed as 100 cm, 125 cm and 150 cm. For this experiment, 60 rock samples from a coal mine located in Westmoreland County in Pennsylvania, were scanned with the mobile LiDAR.

Figure 3.6. *Laboratory experiment set up for classification of lithologies according to the intensity values.*

Figure 3.6 shows the test setup used during experiments. Each sample was placed on a white structure made of boxes. In order to make it easier to recognize the points on the rock samples during the data post-processing, white was chosen as the color of the structure since white objects appear as points with high-intensity values, in contrast to the values obtained from the darker rock samples. A measuring tape was fixed on the table to measure the position of the LiDAR system relative to the rock sample. Three scans were made for each sample by placing the scanner at 100 cm, 125 cm, and 150 cm from the sample. Increasing the distance resulted in a reduction in the number of points obtained for each sample. For example, in the case of a Gray Sandyshale sample, when the LiDAR was 100 cm away from the sample, 2242 points were collected; at 125 cm away, 1693 points were collected; and at 150 cm away, 1318 points were collected. The same duration of scanning, 60 seconds, was applied for all the samples at different distances. Ten samples per lithology were used in the experiments and the following lithologies were considered: Black Shale, Dark Gray Shale, Gray Sandyshale, Dark Gray Sandyshale, Light Gray Sandstone, and Gray Sandstone.

4.0 Research Findings and Accomplishments:

Our research findings and accomplishments are summarized by classifying them into the following categories: (i) evaluate potential for MSHA approval of available low-cost LiDAR technology, (ii) evaluate potential of monitoring rib deformation, movement, or changes from point cloud data, and (iii) evaluate potential for estimation of coal rib lithology from point cloud data.

Potential for MSHA approval of available low-cost LIDAR technology:

The following represents a summary of the considerations for MSHA approval of mobile LiDAR technology units as reported by Kevin Hedrick, an independent consultant contracted for this project.

Introduction

The purpose of this report is to: provide an overview of the Mine Safety and Health Administration (MSHA) approval process; identify MSHA inspections and tests needed to approve a system such as the GeoSLAM Zeb Horizon; identify the potential roadblocks to MSHA approval of the system; and provide recommendations for a company that would design a new system.

The GeoSLAM Zeb Horizon is a handheld LiDAR (Light Detection and Ranging) scanner. The unit consists of the following major components: a handheld laser scanner, a data logger, and an interconnecting cable.

The report is based on a review of: the GeoSLAM Zeb Horizon User Guide Ver 1.1; the Zeb Horizon Specification Sheet; the Velodyne VLP-16 User Manual 63-9243 Rev. D; and MSHA's regulations, policies, and procedures. The author's (Kevin Hedrick's) experience is also relied upon.

Discussion

Overview, MSHA approval process:

The Federal Mine Safety and Health Act of 1977 (30 U.S.C. 801) (Mine Act) (MSHA, 2023a) requires the Mine Safety and Health Administration (MSHA) to establish requirements for the technical design, construction, and testing of electrical products that must be approved by MSHA prior to use in gassy mines. These regulations are divided into separate parts based on equipment type. Title 30 CFR part 18 (part 18) (US National Archives, 2023) specifies the procedures and requirements for obtaining MSHA approval, certification, extension, or acceptance of electric motor-driven mine equipment and accessories intended for use in gassy mines.

MSHA approves, as "permissible," the design of completely assembled electrical equipment, components of electrical equipment, and electrical accessories that manufacturers design, construct, and install to meet MSHA's requirements.

Before electric equipment can be used in gassy mines in the U.S., they must first have been approved for such use by MSHA. Those seeking MSHA approval (applicants) are typically product designers and manufacturers of the equipment or accessories. MSHA's approval process includes testing and evaluation of the products, either by MSHA or by an independent laboratory. Applicants that use an independent laboratory to conduct testing or evaluation must submit the results to MSHA for review, along with written evidence of the laboratory's independence and current recognition by a laboratory accrediting organization.

Technical Considerations: Requirements in part 18, including associated tests, are to ensure that such equipment will not cause a fire or explosion (30 CFR 18.4). Applicants must design electrical equipment so that it will not cause a fire or explosion, using at least one of two recognized methods. One way is to design equipment so that it cannot produce a spark strong enough, or temperatures sufficient, to ignite flammable methane-air mixtures. This protection technique is known as 'intrinsic safety'. As part of this technique, circuitry can be encapsulated in a solidifying material.

Alternatively, applicants may house the equipment in enclosures that will withstand internal explosions of methane-air mixtures without damage to, or excessive distortion of, its walls or covers, and without ignition of surrounding methane-air mixtures or discharge of flame from inside to outside the enclosure. Any interface to circuitry outside of the explosion-proof enclosure would need to be protected against ignition-capable energy.

Administrative Considerations: When MSHA receives an application for approval of a completely assembled electrical machine or accessory for use in gassy mines, MSHA reviews the application using the following steps. First, MSHA examines the documents in the application to determine whether the applicant has met the technical requirements of the provisions of part 18. MSHA also checks each drawing and specification in the application against these requirements and samples of the product or parts of the product. MSHA may disassemble and examine parts of the product for conformity to the drawings and specifications. Second, after MSHA verifies that the product complies with the design and construction requirements, MSHA inspects and tests the product to determine whether the intrinsic safety features perform according to the approval requirements. MSHA issues an approval if the product passes the tests and meets all of MSHA's technical and safety requirements.

Once a product is approved, the applicant becomes an approval holder and must place an MSHA approval marking on the product to indicate that the product is approved for use in gassy mines.

The use of the MSHA approval marking obligates the approval holder to maintain the quality of the completely assembled product according to the technical requirements upon which its approval was based. If an approval holder wants to modify an approved product and maintain its approval, then the approval holder must submit its proposed changes to MSHA. If MSHA approves the changes, the Agency issues either an extension of approval or a notice of acceptance of the modified product to the approval holder.

Documentation requirements, intrinsically safe equipment: MSHA requires documentation that fully describes the equipment. The required types of documentation are Drawings, Bills of Material, and Specifications (MSHA, 2023b). These include: dimensioned assembly drawings; wiring diagrams; schematic diagrams; printed circuit board artwork and layout drawings; and electrical parts lists. Additionally, if lithium-chemistry batteries or cells are used in the design, evidence will be needed to show that they comply with the UL1642 standard (UL LLC, 2023a).

Explosion-proof enclosures: Similar to intrinsically safe equipment, MSHA requires Drawings, Bills of Material, and Specifications that fully describe explosion-proof enclosures MSHA, 2023c. These include, among others: dimensioned assembly drawings; type and grade of enclosure material, including lenses; the size and type of welds; wall thicknesses; flame-arresting path finishes; and the size and grade of bolts.

MSHA Approval inspections and tests:

The GeoSLAM Zeb Horizon system, and similar systems, are designed to be portable equipment. Even the smallest MSHA-certified explosion-proof enclosures are required to be constructed of 1/8-inch steel plate or the equivalent. This typically results in equipment whose weight is above that for equipment that is considered to be 'portable'. It is therefore likely that the system would need to be evaluated per MSHA's intrinsic safety criteria. There are no performance tests of LiDAR equipment necessary for MSHA approval.

As previously noted, MSHA approves the design of the equipment, not the equipment itself. Therefore, inspections are limited to those necessary to prove that the design meets the relevant requirements.

Inspections: Inspections conducted by MSHA before the approval is issued are intended to show that the equipment is built according to the provided design documentation and to facilitate understanding of that documentation. To that end, it is likely that the following samples will be required: a fully assembled system in marketable form; populated and unpopulated printed circuit boards; and three samples of battery packs. MSHA will compare the hardware to the documentation and verify that the electrical (part numbers, resistance, capacitance, inductance, etc.) and mechanical characteristics agree with the documentation. Any deviations between the hardware and the documentation will be noted and provided to the applicant. Those deviations need to be corrected before an approval is issued.

Along with the evaluation of the design documentation, the battery pack will be inspected to ensure that the battery cells are correct and comply with the UL1642 Standard for Safety Lithium Batteries, and are used in compliance with the engineering considerations imposed by the UL1642 acceptance. The distance between the conductive parts of the anode and cathode of the cells will be measured to determine if the cells meet the minimum required separation distances to ensure that an ignition-capable short-circuit cannot occur. If not, the battery pack or portions thereof made need to be encapsulated in an irreversible, solidifying compound. The same separation criteria will apply to interconnecting straps and wires.

Post-approval Inspections may also be conducted to ensure that the equipment is built according to the approval documentation. These inspections may be conducted without the approval holder's knowledge.

Tests: The following describes tests that MSHA could likely conduct on the GeoSLAM Zeb Horizon and its components. Each section describes why the test(s) would be conducted, the conditions of the test, and test procedures. As the details of the circuitry are not known, most of the individual components that would require testing, and the conditions of those tests, cannot be specified.

- *Spark Ignition Test:* If the features of the system cannot be verified to be intrinsically safe based on comparison to MSHA's published spark-ignition curves, spark-ignition tests may be required. Likely candidates for this test are the output of the battery pack, the lumped value of capacitance of the system, and any significant inductive component, such as the motor used in the LiDAR (MSHA, 2023d).

The battery pack of the GeoSLAM Zeb Horizon likely consists of a combination of cells that includes 4 cells in series, as the manual indicates that power supply is 14.8 Vdc. Four cells at a nominal voltage of 3.7 Vdc, when connected in series, will result in 14.8 Vdc. MSHA will consider the voltage of the cells at full charge, not at nominal voltage. For most lithium cells, this is 4.2 V/cell (MSHA, 2023d). This would

result in a pack voltage of 16.8 Vdc. A test factor will be applied; this test factor will most likely be the addition a $\sqrt{}1.5$ factor on voltage, resulting in a test voltage of 16.8 Vdc x $\sqrt{}1.5$ or 20.6 Vdc.

It is assumed that the GeoSLAM Zeb Horizon battery pack does not feature any such current limiting. However, based on assumptions, current-limiting scenarios are discussed in this section.

Based on the open-circuit voltage of 20.6 Vdc, the maximum allowable short-circuit current available from the battery pack would be approximately 2 Adc when referring to MSHA's published spark ignition curve. If the maximum short-circuit current is less than approximately 1.3 Adc, or the value on the '90% curve', no spark-ignition test would be required. The current available from individual batteries or cells would be determined by the Flash Current Test described below. This means that the total series resistance would need to be 20.6 Vdc/ 2 Adc or 10.3 Ω. If a passive current-limiting resistor is used, it will need to be operated at less than 2/3 of its power rating or be tested per *Current-Limiting Resistor Test* described below. To be operated at less than 2/3 of its ratings, this resistor would need to be rated at 61.8 watts or greater (2 A2 x 10.3 Ω x 1.5). Multiple, higher ohmic value resistors connected in parallel could be used, to decrease the power rating of individual resistors, and the resistors could be protected by a suitable fuse(s).

It should be noted that the manual also indicates that the power supply is approximately 1.5 A at 14.8 Vdc. Utilizing passive current-limiting resistance to meet MSHA's requirements would result in maximum nominal short-circuit current of 1.44 Adc (14.8 Vdc/10.3 Ω). The available operating current would likely be somewhat less than that value. This could make the active current limiting more practical.

Active current limiting circuitry would consist of a low-value measuring resistance and utilize non-passive components such as transistors or other solid-state devices that either shunt overvoltage or overcurrent conditions or limit the output of the power source fast enough to prevent an ignition of a methane-air atmosphere. Because these circuits are not included in the list of 'Protective Components or Assemblies', they are considered subject to short-circuit fault; as MSHA applies up to the two worst-case faults, three identical active current-limiting circuits would be required. Testing of active current-limiting circuits is addressed in *Active Current-Limiting Circuit Tests* described below.

The test apparatus consists of counter-rotating electrodes in a mixture of 8.3% methane and air. These electrodes are (a) four tungsten wires and (b) a slotted cadmium disc. The geometry and rotational speed of the electrodes are optimized for the most efficient spark. Either the circuit under consideration or a simulation of that circuit is connected to the apparatus during the test. The sensitivity of the apparatus is verified before and after the test by connecting components that are known to cause ignitions of the test mixture at the lowest practicable energy value. The circuit under test is energized and connected to the test apparatus, the test continues until the test gas is ignited, or for 1000 revolutions of the electrode assembly with the polarity reversed after 500 revolutions. If no ignition occurs, the test mixture is verified upon completion of the 1000 revolutions (MSHA, 2023e).

- *Current-Limiting Resistor Test:* This test is conducted on resistors that are used to limit current to intrinsically safe levels or provide high impedance segregation (decoupling) between two different circuits, if these components would be operated at more than 2/3 of their ratings under normal or fault conditions. These protective components must be metal, metal oxide film, thick film, or of the single layer wire wound type with mechanical protection to prevent unwinding of the wire in

the event of breakage, or any similar construction whose failure mode increases resistance. In the case of a resistor limiting the current from the battery pack in the scenario described for the GeoSLAM Zeb Horizon, the test voltage would be 16.8 Vdc (4.2 Vdc x 4 cells).

Current-limiting resistors are tested up to 1.5 times the maximum fault voltage across the resistor. To be acceptable, the resistor can't decrease in resistance by more than 10 percent, flame, or deform in a manner that could cause a short circuit. The voltage and current are monitored during the tests to calculate the change in resistance value. If the resistor is protected by a suitable fuse, or open circuits during the test, the test is modified to increase the voltage in steps to ensure that the resistor is adequately stressed (MSHA,2023f).

- *Temperature Tests:* Each component operated above its ratings, or identified as a potential source of thermal ignition are tested to determine its maximum surface temperature under worst-case conditions. If the components are housed in a dust-tight enclosure, the maximum allowable surface temperature is the auto-ignition temperature of methane-air mixtures, or 530˚ C. If an enclosure is determined to be not dust-tight, the maximum allowable surface temperature is 150˚ C. The GeoSLAM Zeb Horizon is specified to be "Protection Class IP54." MSHA considers enclosures with Ingress Protection rating of IP5X to be dust-tight, so long as that protection is not compromised by the *Drop Test* described below.

These tests are conducted by connecting samples of the component to the appropriate power source and placing a thermocouple on the surface of the component. The test continues until the temperature becomes constant (MSHA, 2023g).

- *Small Component Thermal Ignition Test:* Components that exceed a maximum surface temperature of 530°C, under normal or fault conditions, during the *Temperature Tests*, described below, are further tested to determine if they present a methane-air ignition risk. MSHA does not define 'small component', so this test is generally conducted on any component or wire that exceeds the 530°C threshold.

The test mixture of 7.7% methane-in-air is introduced into a test enclosure. The test mixture is verified by placing a wire of known characteristics in the enclosure and applying adequate current to cause an ignition. The component under test is then placed in the enclosure and energized under the conditions that give the maximum surface temperature. The test continues until the temperature becomes constant, or the test mixture ignites (MSHA, 2023h).

- *Flash Current Test:* This test is designed to determine the internal dc resistance of batteries. The GeoSLAM Zeb Horizon includes lithium batteries of unknown type and quantity; samples of these batteries would be subject to this test.

In this test, a conditioned and fully charged battery is connected in series with a mercury switch and a precision non-inductive 0.1 Ω 50-watt (minimum) resistor using low-impedance wiring. An oscilloscope is connected across the load resistor, and the voltage across the resistor is monitored and recorded. The peak voltage after 20 μsec is noted, and used to calculate the current through the resistor. The internal resistance is then calculated by dividing the open circuit voltage of the battery by the current through the resistor, and then subtracting the 0.1 Ω value of the test resistor. The open circuit voltage of the battery is

then divided by the calculated internal resistance value to determine the maximum short-circuit current capability of the battery (MSHA, 2023i).

- *Drop Test:* MSHA conducts drop tests of portable apparatus to ensure that the enclosure remains dust tight and that no significant damage is likely due to the rough use environment of an underground mine. Some features of intrinsically safe equipment need to be segregated by spacing; these distances are (a) measured across surfaces, such as printed circuit boards and are called creepage distance, (b) through air and are called clearance distances, and (c) distances through solid insulation or casting compound. If the enclosure is determined to be not dust-tight, then the spacing requirements are considered to be not met. The handheld portion of the GeoSLAM Zeb Horizon and the battery pack would be subject to separate drop tests.

A sample of each component is dropped six times from a height of 3 feet onto a one-inch-thick oak plank. Each drop is intended impact onto a different surface of the apparatus. After the test, the components are inspected for significant damage. If a visual inspection is not sufficient, additional testing may be conducted to ensure that the enclosure is dust-tight (MSHA, 2023j).

- *Coal Dust Thermal Ignition Test*: This test would be conducted only if an internal component of the system is subject to a coal dust layer because the enclosure is not dust-tight, and the component has been found to exceed 150°C in the temperature test described in *Temperature Tests* below.

A sample of the component is placed in a test enclosure and a thermocouple is attached to the component. A second thermocouple is placed 0.25 inches above the component, and fine coal dust is placed on the component to a depth of 0.5 inches above the top surface of the component. Power is applied to the component such that the maximum surface temperature is obtained. Ignition of the coal dust is a failure of the test; ignition is indicated if the temperature 0.25 inches above the component is higher than the surface temperature of the component or by visual observation (MSHA, 2023k).

- *Encapsulation Test:* Portions of the circuitry may be encapsulated to ensure separation between conductors and components, to ensure connection of protective components to piezoelectric or energy storage components, to protect fuses that might be an ignition risk if broken, or reduce surface temperatures. If so, these are subject to a force test of 30 N with a 6 mm rod for 10 seconds (MSHA, 2023l). It's unknown if any of the components of the GeoSLAM Zeb Horizon are encapsulated for any of those purposes.

If any of the circuitry is encapsulated to exclude explosive mixtures of methane and air from its components, a separate test program is indicated as discussed in *Encapsulated Assemblies* below.

- *Piezo-Electric Component Test*: Piezoelectric components convert electrical energy to motion, or mechanical stress to electrical energy. The GeoSLAM manual indicates that pressing a button can result in "beeps." It is unknown if the beeps are generated by a piezoelectric component or an electromechanical speaker. If it is piezoelectric, MSHA will conduct a test to ensure that impact to the component in its intended mounting will not result in 1500 μJ of energy.

Samples of a piezoelectric component are mounted in a fixture, and 20 J impact energy is imparted by a 5 lb. test mass with a 1-inch hemispherical impact head. The method used is either with the mass at the end of a pendulum swinging through 90° or the mass is allowed to fall vertically with a drop of 36 inches.

The voltage generated by the component is measured, and the capacitance value at its output leads is measured. The energy is then calculated (MSHA, 2023m).

- *Active Current-Limiting Circuit Tests:* As noted above, it is assumed that the GeoSLAM Zeb Horizon battery pack does not include requisite current limiting. This section provides an overview of active, non-linear circuitry is used for that purpose. Active current limiting can allow for better operation than using passive resistance; the full voltage is available up to the current trip point. However, MSHA subjects active current-limiting circuitry to intensive testing and measurement (MSHA, 2023n). Spark ignition tests are conducted on safety-factored and non-safety-factored circuits. A minimum of 4000 short-circuit sparks (when the tungsten wire contacts an edge of the cadmium disk) and 4000 open-circuit sparks (when the tungsten sire leaves an edge of the cadmium disk) are part of the test program. Spark ignition testing is conducted with the appropriate load capacitance. Depending on the method used by the active circuitry, MSHA may devise additional testing.
- *Encapsulated Assemblies*: These tests are conducted on circuits that use encapsulation to provide safety by separating potential ignition sources from potentially explosive atmospheres. It is unknown if the GeoSLAM Zeb Horizon uses has any encapsulated circuits. However, the system uses a LiDAR sensor that could be similar to the Velodyne VLP-16. The Velodyne manual states "(f)or various reasons, you may wish to encapsulate the sensor, either wholly or partially." It is not known if the sensor and other circuits of the GeoSLAM Zeb Horizon could benefit from this form of encapsulation.

Because there are parts that need to rotate, encapsulation of the interior of the sensor is not indicated. The sensor could be encapsulated with the interior remaining as an unencapsulated free space, noting that MSHA does not allow free space in excess of 10 cm3 inside an encapsulated assembly.

The Velodyne manual indicates that the power for the VLP-16 should be 9-18 Vdc, "drawing a maximum of 0.9 A during normal operation" and "(t)he power source must be capable of providing as much as 3.0 A to accommodate the current surge that occurs during rotor spin-up when power is supplied to the sensor. In normal operation the sensor draws approximately 8 W of power." This suggests that the motor is the most problematic component in the sensor; if the motor does not pass a spark ignition test, encapsulation of the sensor is a possible solution. The energy at the terminals of the sensor would need to be intrinsically safe.

MSHA's encapsulation criteria (MSHA, 2023o) is divided into two sections, one of which deals with encapsulated circuitry that is non-incendive in normal operation, and another that covers encapsulated circuits and devices that are incendive in normal operation. In this context, incendive means "able to release enough electrical or thermal energy to ignite a flammable mixture of the most easily ignitable composition of methane and air." Normal operation means that "operation of apparatus conforming electrically and mechanically within its design specification and used within the limits specified by the manufacturer and MSHA-defined conditions of use, application of the worst-case non-countable faults and normal operating conditions as stated in ACRI2001." If the equipment is deemed to be 'incendive', the encapsulation requirements are more onerous; for example, the minimum thickness of the material is greater.

The tests required for encapsulated assemblies are generally the same for 'incendive' and 'non-incendive' circuits. These tests are:

- The force test, described in *Encapsulation Test* above.
- Encapsulation compound is required to adhere to any object, such as a cable, protruding from the encapsulated assembly and ensure against the possible entry of moisture or hazardous gases through this seal. The seal is verified by hanging a weight equal to 5 time the mass of the assembly from the cable for an hour and inspecting for failure of adhesion (MSHA, 2023p).
- Encapsulation compounds, when cured, are required to be non-permeable. Permeability is determined by submersion in water for 24 hours, and comparing the post-submersion weight with the pre-submersion weight (MSHA, 2023q).
- The encapsulation compound is required to be resistant to changes in temperature. A sample of the encapsulated assembly is maintained at a high temperature at 90% relative humidity for 4 weeks and then at a low temperature (-25°C) for 24 hours. The high temperature is determined by the evaluation, but is at least 80°C. A visual inspection then determines if there is any damage that would comprise the protection of the encapsulant (MSHA, 2023r).
- Testing is conducted on the free surface of encapsulated assemblies to determine if there is protection against damage from impact. This testing is the same as *Encapsulated Assemblies Test*.
- Samples of encapsulated assemblies are subjected to drop testing similar to that described below in *Drop Test*; no damage is allowed that would affect the isolation of the assembly from the hazardous atmosphere (MSHA, 2023s).

Potential Roadblocks to MSHA Approval: When developing this section, an internet search was conducted to discover any LiDAR equipment approved for use in explosive atmospheres. The intention of this search was to determine if there was any LiDAR equipment approved in other countries, and, if so, was that equipment approved for use in mining environments and what protection techniques were used. The following two units were found.

- *ExRobotics B.V Model LDR-SW-003226:* This is a module that is intended solely for use on ExRobotics' EXR-2 autonomous inspection robot (ExRobotics B.V., 2023). This a track-driven mobile robot designed for safety inspections of industrial environments. The internationally-accepted IECEx certificate (UL LLC, 2023b) for the module indicates that it housed in a flame-proof enclosure (similar to MSHA's explosion-proof enclosures) for use in non-mining applications. Furthermore, it is accepted for use in Zone 1, which designates that the equipment would be exposed to hazardous gas occasionally. MSHA's intrinsic safety approvals are more similar to Zone 0, where the exposure is assumed to be constant and the equipment can remain energized in the explosive environment.
- *Z+F IMAGER® 5006EX explosion-proof 3D laser scanner*: This is a fixed laser scanner that appears to be intended to be mounted on a tripod (Zofre, 2023a). This is not a portable unit; it weighs 30.6 kg. It is certified (Zofre, 2023b) in Europe per the EU's ATEX directive for use in both mining and non-mining applications. The mining certificate indicates that it is flameproof enclosure and the optical radiation is acceptable for the environment. It is also accepted for use in Zone 1 and not Zone 0. It would be required to be deenergized in the presence of explosive mixtures of methane and air.

- *MSHA-approved equipment:* There are no portable LiDAR units approved by MSHA. However, the basic technologies (Class I lasers, small motors, IR detectors, electronic circuits, lithium batteries) have been features of various MSHA-approved portable equipment. There are no roadblocks based on the underlying technologies of equipment such as the GeoSLAM Zeb Horizon.

Administrative Considerations:

- *Market size:* Although this subject is outside of the author's expertise, he has anecdotal evidence from several decades of discussions with manufacturer's representatives that the market size for specialized equipment for use in underground mines is small compared to the costs. Magison (1998) notes that "(i) intrinsic safety design increases costs. Added components increase unit cost. Added design time increases development costs." It can cost tens or hundreds of thousands of dollars to redesign and manufacture a product to meet MSHA intrinsic safety requirements. Sales of the product need to be proportionate to recoup those costs. The author is unaware of the size of the market for a portable LiDAR unit in gassy underground mines in the United States, but it would certainly be smaller than the market for intrinsically safe equipment that is already in widespread use.

Also related to the market for this equipment, approved equipment is not modified or updated on the same schedule as most consumer equipment or some other industrial equipment. Because MSHA controls the documentation of approved equipment, and any modifications need to be evaluated by MSHA, the designs tend not to be modified frequently.

- *Documentation not available:* MSHA requires "drawings, drawing lists, specifications, wiring diagram, and descriptions shall be adequate in number and detail to identify fully the complete assembly, component parts, and subassemblies." (MSHA, 2023b) It is likely that components of the system, such as the LiDAR sensor and USB stick, are manufactured by entities other than the assembly of a product such as the GeoSLAM Zeb Horizon. Those manufacturers may be protective of their intellectual property and be unwilling to share the documentation with the applicant. MSHA will not issue an approval without that documentation.

MSHA has a program (MSHA, 2023t) to allow a third party to submit documentation directly to the government; in that case, MSHA assures the confidentiality of the documentation submitted by the subassembly manufacturer. The drawings submitted to MSHA by the subassembly manufacturer will be filed at MSHA as part of the investigation and identified on the drawing list sent to the applicant. However, the third-party manufacturers may not wish to share that documentation with MSHA.

- *Equipment not designed for use in methane-air mixtures*: If a manufacturer submits to MSHA a design for a product where intrinsic safety has not been part of the design process, it is likely to be rejected. For a product such as the GeoSLAM Zeb Horizon, that is the most likely outcome if the existing design is submitted to MSHA. In that scenario, MSHA will provide a list of discrepancies between the design and their requirements, and allow the applicant a reasonable time to address all of the discrepancies (MSHA, 2023u). If more time is required, the application would be canceled and fees for the evaluation time would be charged.

Technical Considerations: It is almost certain that the GeoSLAM Zeb Horizon was not designed for intrinsic safety in underground mines or any other environments. It is impractical to house the components in explosion-proof enclosures as the increase in weight would cause the system to no longer be portable. The following are some of the implications of an intrinsic safety design.

- *Increased Weight and Size:* Even though the components would not be housed in explosion-proof enclosures, there would likely be increases in the mass of its components. For example, additional weight could be due the additional components needed to limit the current from the battery pack. Portions of the circuit may need to be encapsulated or coated. Components may need to be added to the circuit to ensure intrinsic safety, such as additional resistance, optical isolators, or diodes across inductive components. The spacing between components and conductors may need to be increased. The enclosures may need to be strengthened.
- *Functional issues:* The basic premise of intrinsic safety is limitation of energy. This requires various voltage- and current-limiting techniques. Magison (1998) states that "alteration to circuits imposed by intrinsic safety compromise the functions desired in the product or make it much more difficult to achieve the desired function at the target investment, project completion date, or unit cost." Some of the compromises for a portable LiDAR system include decreased runtime and decreased performance due to restrictions on power.

Recommendations for Design of a New Portable LiDAR System:

These recommendations are intended for those who wish to design and manufacture a portable LiDAR system for use in gassy underground mines in the United States. It is not intended to be a primer for design personnel but does give guidelines.

Those companies that routinely apply for MSHA approval of their equipment utilize in-house expertise for the intrinsic safety aspects of the equipment or rely on outside agencies. Magison (1998) provides a roadmap for this process. He says that a design project for intrinsically safe or associated apparatus must include the following tasks. Work will progress in general from one step to another; however, the process, like any other design process, is usually an iterative one; partially completing a step, proceeding to the next step or two, and then looping back through the steps with more focus on detail.

Establish the Intrinsic Safety Design Objective: The designer should ask: Is intrinsic safety needed in all models, or should it be an add-on option? The documentation and technical requirements should be reviewed before the design process begins. If in-house expertise for intrinsic safety does not exist, it may be beneficial to engage with an outside agency at this point.

- *Design the Product:* Designing intrinsic safety into a product must occur as the schematic is drawn. It should be an ongoing consideration from the first attempt to draw the schematic because there are always several ways to achieve intrinsic safety. These choices should be traded off against the effect on function, cost, and even the size or number of layers of the printed circuit board. Intrinsic safety considerations are often taken into account only after a nearly final functional schematic has been drawn. The designer then passes the schematic to the intrinsic safety specialist, who adds components needed to ensure intrinsic safety to the schematic and writes down the spacing rules. This procedure robs the design of the benefits of tradeoffs between the functional design, cost, and so on, and usually is used when the circuit design people do not want to assume any of the

responsibility for making the design intrinsically safe. The result is almost certain to be a less-well-optimized design.

The first item associated with a portable LiDAR system such as the GeoSLAM Zeb Horizon that should be designed for intrinsic safety is the battery pack. Almost all other electrical aspects of the system will rely on an intrinsically safe power supply. As discussed in more detail in *Spark Ignition Test*, the values of voltage and current should be computed and compared against the MSHA's requirements.

The values of voltage and current in the remainder of the circuitry under normal and with up to the two worst-case faults should be determined, and along with the values of capacitance and inductance, compare to MSHA's requirements. Then, the designer should identify constraints on layout, materials, and component ratings that are implicit or explicit in the previous steps.

MSHA provides limited guidance in a document titled "Understanding and Expediting the MSHA Intrinsic Safety Approval Process - Frequently Asked Questions and Guide." (MSHA, 2023v) This document provides answers to frequently asked questions by applicants seeking MSHA approval or evaluation of intrinsically safe apparatus and associated apparatus, and addresses the most common problem areas encountered in approval applications. Additionally, 30 CFR part 18 allows applicants or their representatives consultations to discuss a proposed design to be submitted for approval at no charge; it is recommended that applicants take advantage of this opportunity.

- *Document the design for MSHA to save time and money by easing the evaluation and approval process*: When documenting the design, an applicant for MSHA approval should ensure that the documents are complete and provide the detail required by MSHA. Some applicants maintain an approval documentation package that may differ from the manufacturing documentation. This package provides only those details needed for MSHA approval and highlight the intrinsic safety features of the design (MSHA, 2023c).
- *Document the design in manufacturing drawings, specifications, and inspection procedures*: This is intended to make it easy to control the details relevant to intrinsic safety and its certification throughout the life of the design. As Magison indicates, the objectives of this step are as follows: (1) Ensure that assumptions made in the intrinsic safety analysis and the claims made on the certification drawings are supported by the documents used to procure components and manufacture parts and assemblies; and (2) Put in place those inspections and audits needed to ensure that the features pertinent to the approval appear in the product, as called for in the manufacturing drawings and specifications, and as required by the certification documentation.

MSHA will require the applicant to provide a factory inspection form (MSHA, 2023c); alternatively, it will accept a document signed by a company official stating that the company will conduct regular inspections of all MSHA approved devices manufactured by the company to ensure that the products are made and assembled in strict accordance with the drawings and specifications approved by MSHA.

Potential of monitoring rib deformation, movement, or changes from point cloud data:

The objectives of the first and second field experiments, detailed in section 3 under research task 2, are to evaluate the potential of monitoring rib deformation or changes. The findings from these experiments are reported here.

Experiment #1:

In the first experiment, seven rock pieces of different sizes were placed on the floor of the coal mine entry to artificially induce rock falls. The coal mine entry was mapped with mobile LiDAR before and after inducing rock falls. Then, LiDAR data was processed with GeoSLAM Hub and CloudCompare's ICP and M3C2 algorithms to compare before and after point clouds to identify the changes.

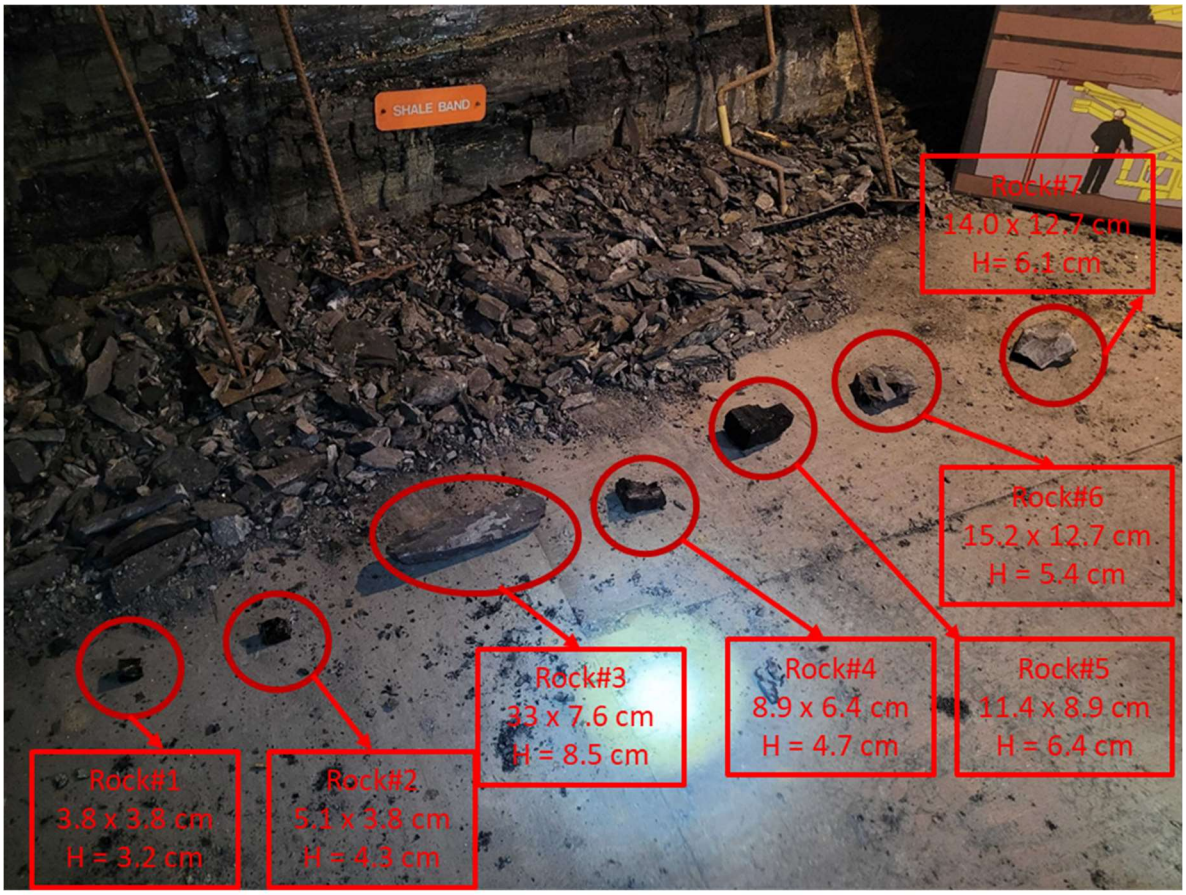

Figure 4.1. *Seven rock pieces, representing induced rock falls, and their width and length dimensions.*

Figure 4.1 shows the seven rock pieces and their dimensions. The smallest rock is 3.8 cm in width and 3.8 cm in length, and the largest rock is 33 cm in length and 7.6 cm in width. Therefore, when we compare the point clouds before and after inducing the rockfalls and calculate the changes between them, in an ideal condition, we would expect to see the seven rock pieces that we placed on the floor. However, due to the measurement errors caused by the imperfection in any surveying instrument and environmental factors, and computational errors caused by the assumptions inherent to the numerical solution methods, there is a limit to the accuracy of the changes computed. The smallest rock piece that we can see, after applying the algorithms, is representative of the precision of this equipment, with the associated algorithms applied, to detect changes in the environment in which the surveys were performed.

Another important factor in the evaluation of the change detection accuracy is the number of traverse loop closures performed with the mobile LiDAR equipment. SLAM algorithms apply corrections, similar to the error of closure in boundary surveying, to the local map and estimated location of the equipment. Therefore, as the operator surveys the environment with more loop closures, both local map accuracy and

point density on the rib surfaces increase, which would also improve change detection capabilities. To evaluate the effect of the number of loop closures on the change detection accuracy: (i) Before rock falls were induced, the coal mine entry was surveyed two times with one loop and two loops of closures with mobile LiDAR. (ii) After rock falls were induced, the coal mine entry was surveyed three times with one, two and three loops of closures. Table 4.1 shows the acronyms used for identifying each survey, and acronyms are found necessary to reduce the number of words used to identify specific surveys in the text and figures.

Table 4.1. *Acronyms used in the report for identifying each survey.*

Number of Loop Closures	*Before Rock Falls Induced*	*After Rock Falls Induced*
1	S-1L-A	S-1L-B
2	S-2L-A	S-2L-B
3	-	S-3L-B

Figure 4.2 shows a photo and 3D point cloud map of the test environment. Some of the landmarks are marked with dashed red circles.

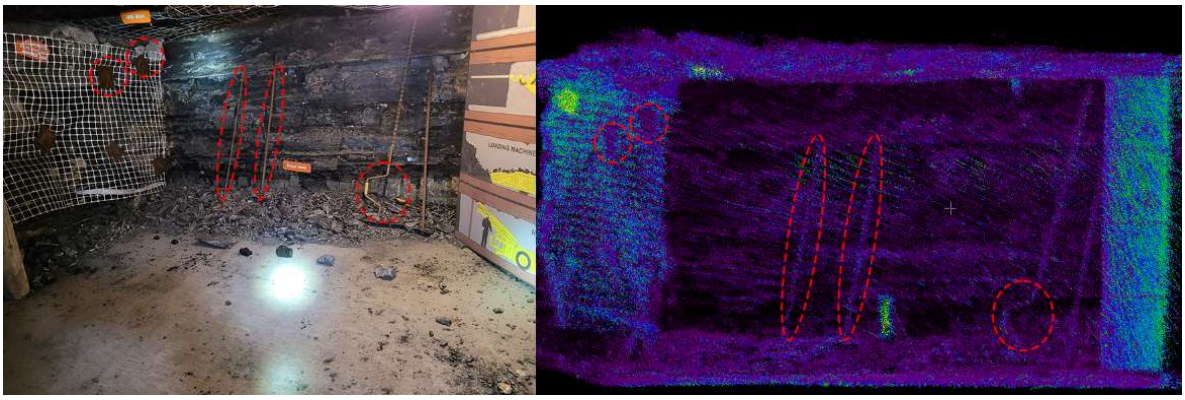

Figure 4.2. *Photo and 3D point cloud map of the field experiment#1 survey environment.*

After the LiDAR surveys, data (point clouds) were compared, and the distances between them were computed using the M3C2 algorithm. Figure 4.3.A shows the initial visualization of the distances between the S-1L-A and S-L1L-B point clouds as a 3D color plot. Distances between the point clouds were computed along the vertical direction (z-axis). In this comparison, S-1L-A is the reference point cloud, so positive distances indicate material added on the surface of S-1L-B or change of a surface in a positive vertical direction (up or +z axis), and negative displacements indicate material removed from the surface of S-1L-B or change of a surface in the negative vertical direction (down or -z axis).

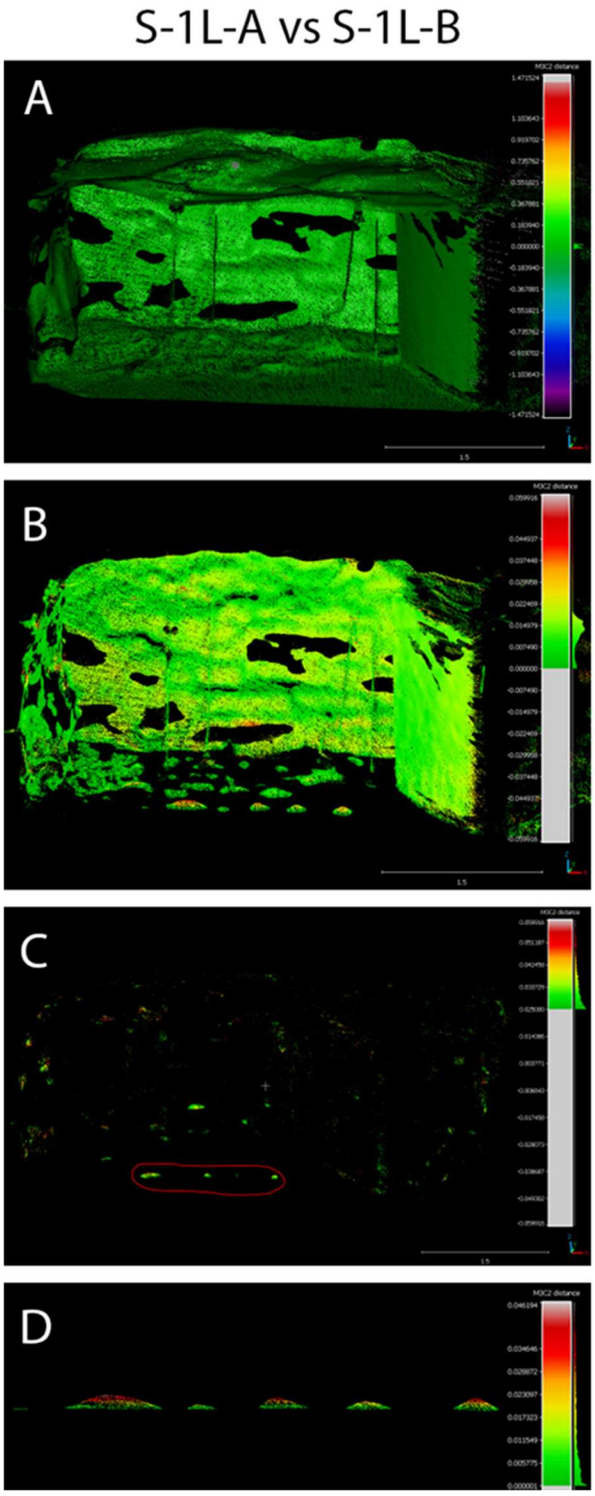

Figure 4.3. *Vertical distance between S-1L-A and S-1L-B point clouds and filtering of color legends A) Default, B) 0 – 6 cm, C) 2.5 – 6 cm, D) 0 – 4.6 cm.*

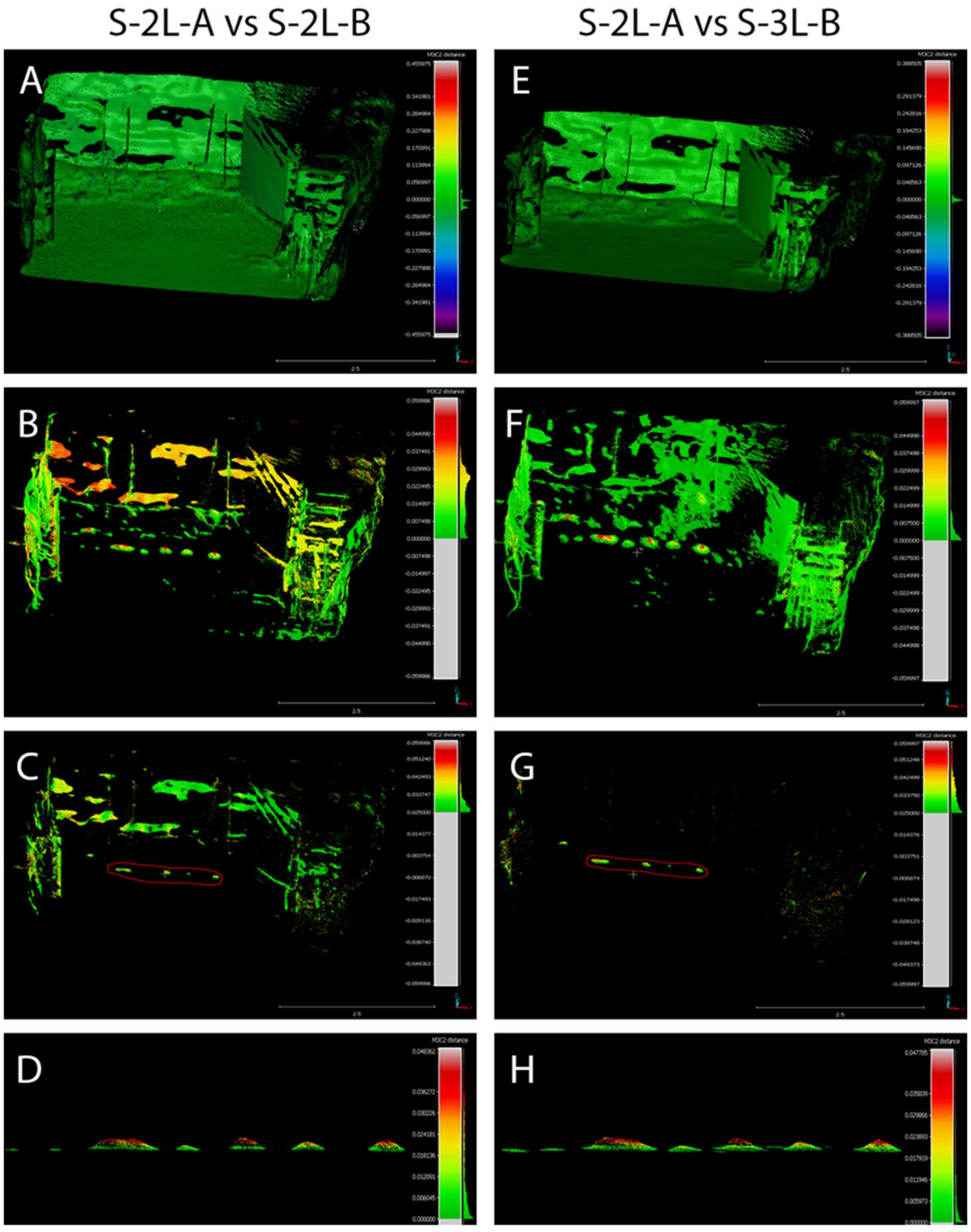

Figure 4.4. *Vertical distance between S-2L-A and S-2L-B (A to D), S-2L-A and S-3L-B (E to H) point clouds and filtering of color legends A) Default, B) 0 – 6 cm, C) 25 – 6 cm, D) 0 – 4.6 cm, E) Default, F) 0 – 6 cm, G) 2.5 – 6 cm, H) 0 – 4.6 cm.*

Figure 4.3.A shows that displacements of the surface points are near zero (green color according to the color legend). Due to the noise in the data, maximum and minimum values of the color legend are set between 1.5 m to -1.5 m as a default by the program. Therefore, noise has to be filtered from the color plot by adjusting the max and min values of the legend. In 4.3.B, since it is expected that changes to be positive, the minimum value of the color plot is set to 0.0 (zero) and the maximum is set to 6.0 cm. In this plot rock pieces on the floor are visible, but noise still exists. Since the changes in the vertical direction are compared by comparing the vertical distance between the point clouds, noise on the floor should be removed. In 4.3.C, the legend ranges from 2.5 cm to 6.0 cm, and most of the noise on the floor is removed. Larger size rocks (#3, #5 and #7) are visible (inside the red circle in 4.3.C), but hard to distinguish from the view. Figure 4.3.D shows the view of the rock pieces when zoomed into their location and the legend ranged from 0 to 4.6 cm. We can see all the rock pieces except the smallest one, rock #1.

Figures 4.4.A to 4.4.D show the comparison of the point clouds S-2L-A and S-2L-B, and Figures 4.4.E to 4.4.H show the comparison of the point clouds S-2L-A and S-3L-B. The same filtering procedure described above was used for these two comparisons as well. When Figure 4.4.G is compared to Figures 4.3.C and 4.3.D, as the number of loops increases, the possibility to identify the differences between point clouds increases. When two and three loops were traversed, one more rock (#6) was identified (Figure 4.4.C and 4.4.G), compared to the single loop case. In addition, Figures 4.4.D and 4.4.H show the view of the rock pieces when zoomed to their locations for two and three loops of traverses. All seven rocks are visible compared to the point cloud generated from the traverse of one loop.

The following research findings were derived from the results of the first experiment: It is possible to detect changes, as rock falls from ribs or roofs, from mobile LiDAR measurements. In this study, the size of the smallest change, reliably, that the GeoSLAM Zeb Horizon LiDAR system detected is concluded as approximately 6.0 cm (Figures 4.3.C, 4.4.C and 4.4.G). However, as the number of loops traversed increases, noise in the data decreases and the reliability of the change detection also increases. These results also depend on the algorithms used in this study and the type of LiDAR. Zeb Horizon uses Velodyne VLP-16, 16-channel LiDAR, and a 64-channel LiDAR would be expected to allow detection of the smaller changes.

Experiment #2:

In the second experiment, rock pieces from the coal pillar rib were removed to artificially induce changes on the rib. The coal mine entry was mapped with mobile LiDAR before and after inducing changes on the rib, and three loops of traverses were performed in each survey. In this experiment, I-site 82000 static LiDAR scanner was also used to map the entry before and after inducing changes. Dr. Brent Slaker and Nicole Evanek from PMRD/NIOSH performed the I-Site 8200 survey and provided the raw point cloud data to CSM/WVU team. Then, LiDAR data was processed with GeoSLAM Hub and CloudCompare's ICP and M3C2 algorithms to compare before and after point clouds to identify the changes on the rib.

Figure 4.5 shows the horizontal distances computed by the M3C2 algorithm for point clouds mapped by mobile and static LiDARs before and after inducing changes and the filtering of the results. The results indicated that change on the rib couldn't be identified from the mobile LiDAR data since the induced change is less than 6 cm (Figures 4.5.B and 4.5.C). There are trances of change, but it is not possible to distinguish them from the noise. On the other hand, the changes on the rib can be identified from the static LiDAR results (Figures 4.5.E and 4.5.F). I-Site 8200 can produce denser point cloud data compared to

Zeb Horizon, and the changes computed by the I-site 8200 scanner are in the 2.0 to 3.5 cm range. From the first experiment, we can conclude that it is hard for Zeb Horizon to identify changes under 6 cm. Results of the second experiment also confirm that the type of LiDAR used in the system is an important factor in the accuracy of the changes that can be detected.

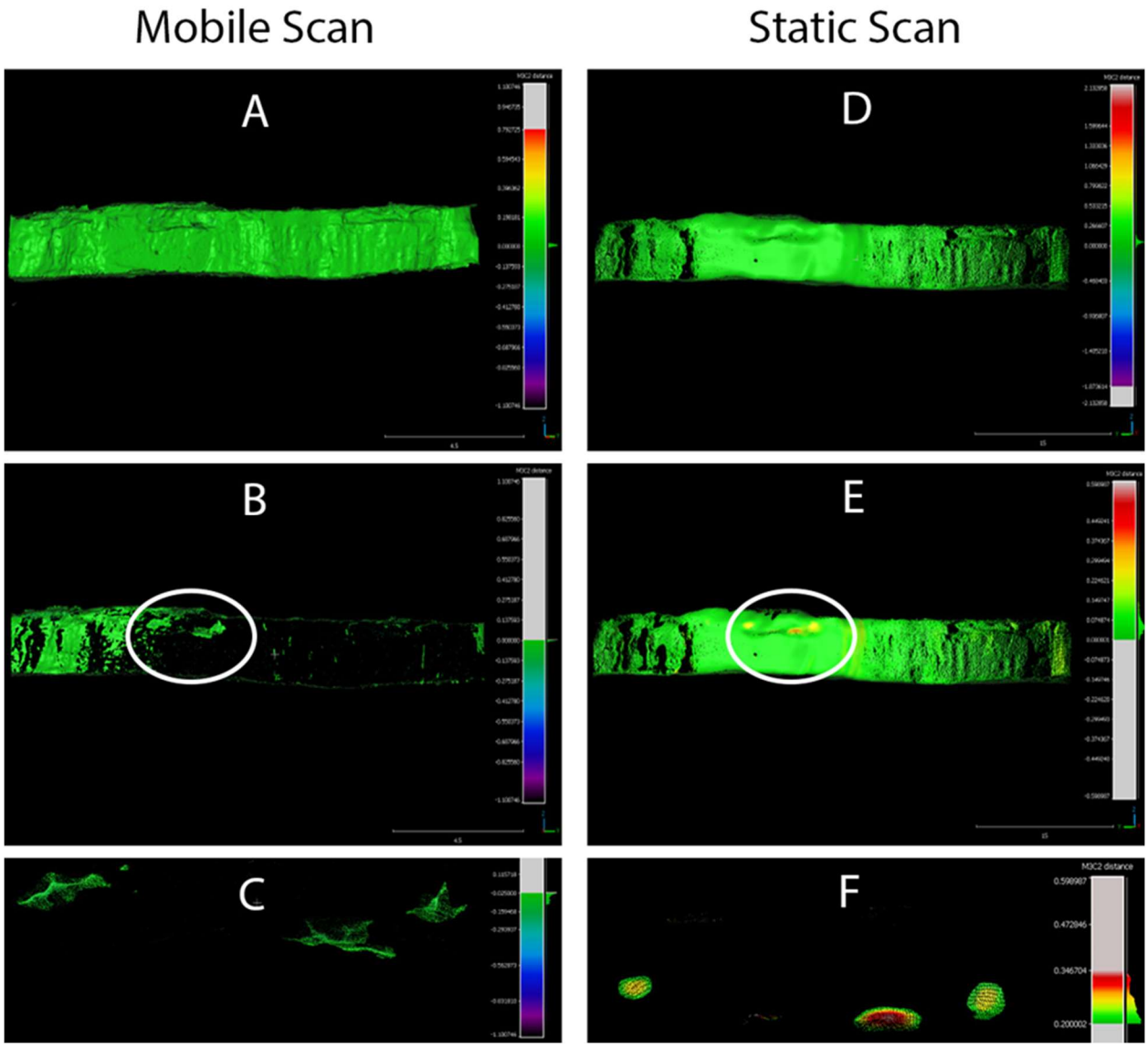

Figure 4.5*. Sequences of filtering. Mobile Scan: A) Default, B) 0 – 110 cm, C) 2.5 – 110 cm. Static Scan: D) Default, E) 0 – 6.0 cm, F) 2.0 –3.5 cm.*

<u>Potential for estimation of coal rib lithology from point cloud data:</u>

Intensity values provided by the LiDAR scanner represent a promising data source for discrimination of different lithologies. These values are the amplitude of the return signal, which represent the analog electrical signal output from the photodetector or the digitized waveform (Kashani et al., 2015). The amplitude then is scaled to an 8-, 12-, or 16-bit dynamic range so that it can be converted to a number that

is a parameter in a point cloud. Depending on the LiDAR system, the intensity value might have different intervals according to dynamic range scale. For example, an 8-bit dynamic range is from 0 to 255; for 12-bit, from 0 to 4095; and for 16-bit, from 0 to 65535.

In this research, it was demonstrated that SLAM-based LiDAR can be used to recognize the changes in the lithology from the intensity values. LiDAR measurements of rock cores from various lithologies were first gathered in a lab setting to examine the link between the lithology, the intensity values, and the measurement distance. The LiDAR data was processed with Cloud Compare, and One-Way ANOVA was used to compare the intensity values obtained for each lithology. Then to validate that the intensity values can be utilized to estimate the lithology of a coal rib in the field as well, the data from the third field experiment (Section 3.0, Research Task 2, Experiment #3) was analyzed.

Laboratory Experiments:

Ten samples were imaged per lithology (except for coal; only three samples were available) and three sets of LiDAR measurements were made for each sample. Python scripts were developed to analyze the data obtained in laboratory experiments. The pandas and NumPy libraries were used for the analysis of LiDAR data, and the seaborn library was used for data visualization. To represent each test category with a simpler representative identification during the data analysis and in the test, tables and graphs, acronyms were used to represent each test category. Table 4.2 summarizes the acronyms selected to represent each test category.

Table 4.2. *Acronyms used in the report for identifying each laboratory experiment category.*

Color of the Sample Rock and Representation		*Lithology of the Sample*		*Distance between LiDAR and Sample*	
Black	B	Shale	SH	100 cm	A
Dark Gray	DG	SandyShale	SDS	125 cm	B
Gray	G	Sandstone	SD	150 cm	C
Light Gray	LG	Coal	CL	-	
Example: Black Shale 125 cm from the LiDAR = B_SHB					

Each sample, depending on its size, distance from the LiDAR, and the duration of LiDAR measurement, is represented as a point cloud with a different number of points. For each lithology, measured data from each sample (belongs to a specific lithology) were grouped together as the representative point database for that specific lithology. Table 4.3 shows the size of the point database for each case. As the distance between the LiDAR and sample increased, the number of points slightly decreased. Also, stronger rock types (i.e., gray sandy shale or sandstone) generally have larger physical sample dimensions, hence a larger number of data points. Since it was harder to gather intact coal samples from the core, the number of coal samples and their sizes were the smallest, which is why there are lower numbers of points in the coal group.

Table 4.3. *Point database size for each lithology.*

Lithology Group Name	*Distance from the LiDAR*		
	A (100 cm)	*B (125 cm)*	*C (150 cm)*
Black Shale	*19414*	*15348*	*11648*

Dark Gray Shale	*26296*	*22008*	*16872*
Dark Gray SandyShale	*23181*	*22008*	*16872*
Gray SandyShale	*33130*	*26722*	*19514*
Light Gray Sandstone	*33636*	*30785*	*23721*
Gray Sandstone	*26193*	*25951*	*18360*
Coal	*2785*	*2560*	*1997*

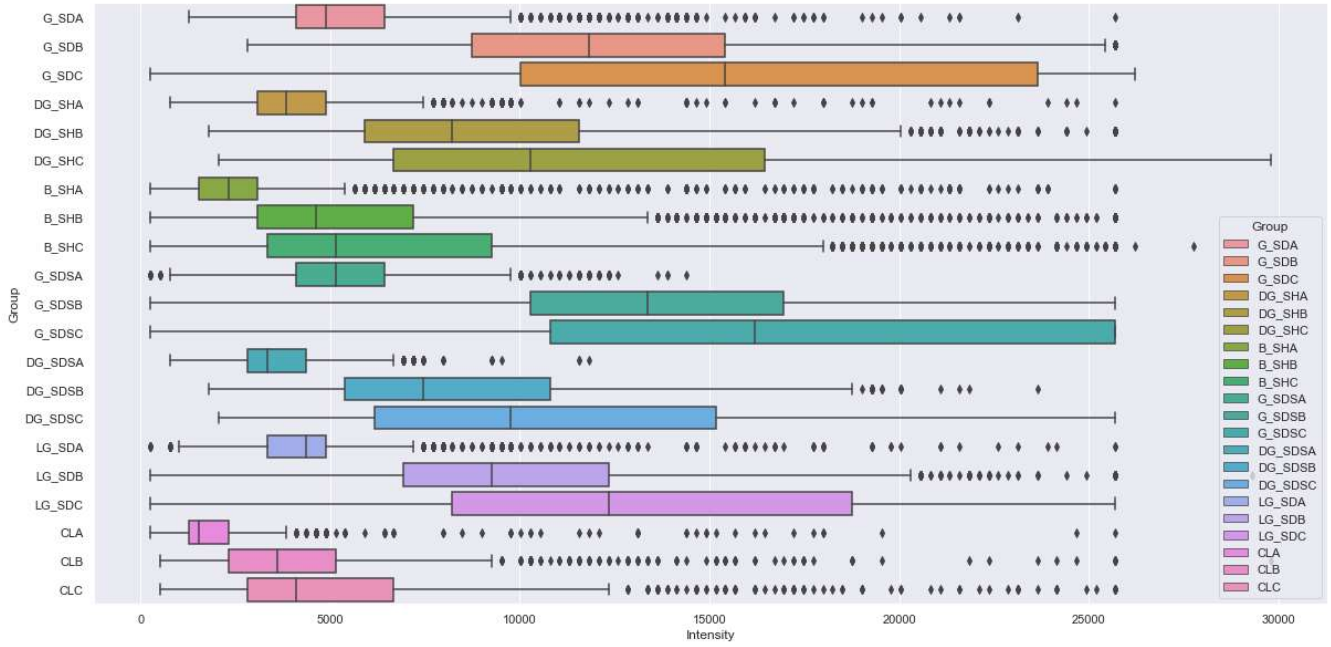

***Figure 4.6**. Boxplot visualization of the whole database.*

Figure 4.6 shows the boxplot visualizations of the whole database categorized by each lithology group. The horizontal axis is the intensity value, and the vertical axis is the lithology and distance categories. A box plot visualizes the distribution of numerical data in a way that makes it easy to compare categorical variables. The first observation from the visualization of the data is that as the distance between the LiDAR and sample increases, median and variance also increase. Literature review and communications with GeoSLAM indicated that different filters are used to enhance or reduce the intensity according to the distance from the scanner to the target (Matasci et al., 2015), which theoretically implies that distance shouldn't affect the intensity value distribution parameters, median or variance, significantly. Further communications with GeoSLAM staff revealed that there is a scaling curve applied to ZEB Horizon intensity values when the distance to the surface is larger than 2.0 meters. Due to the proprietary nature of applied scaling curve, we couldn't include this information in our research report. However, application of a scaling curve after 2.0 m distance measurements indicate that to evaluate the potential of separating lithologies based on intensity values, lithology groups in each distance group should be evaluated separately.

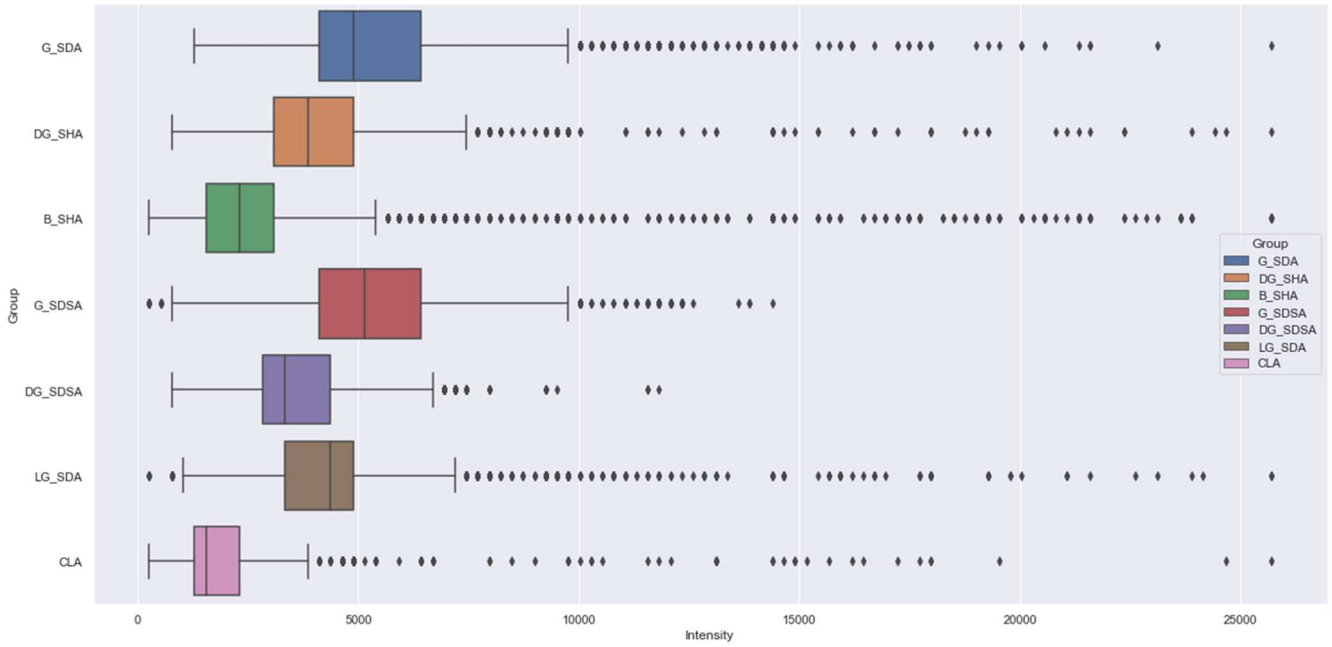

Figure 4.7*. Boxplot visualization of the point database when distance between LiDAR and sample was 100 cm.*

Figure 4.7 shows the boxplot visualization of the point database of the lithology groups when the distance between LiDAR and samples was 100 cm. Results clearly indicate that Coal (CLA) can be separated from Dark Gray Shale (DG_SHA), Gray Sandyshale (G_SDSA), Dark Gray Sandyshale (DG_SDSA), Light Gray Sandstone (LG_SDA) and Gray Sandstone (G_SDA) from the intensity values. However, it isn't possible to conclude a similar result for the Black Shale (B_SHA). Figure 4.8 shows the visualization of the point database of the lithology groups for LiDAR – sample distance of 125 cm and, Figure 4.9 shows for the distance of 150 cm. The same conclusions can be derived from these two visualizations as well: intensity values can be used to separate the coal from Shale and Sandstone lithologies, except for the Black Shale. Even though the visual information of the boxplots is useful and might even be used to determine if two lithologies have different values from each other, statistical analysis is necessary to reliably state that one group is different than others (or not).

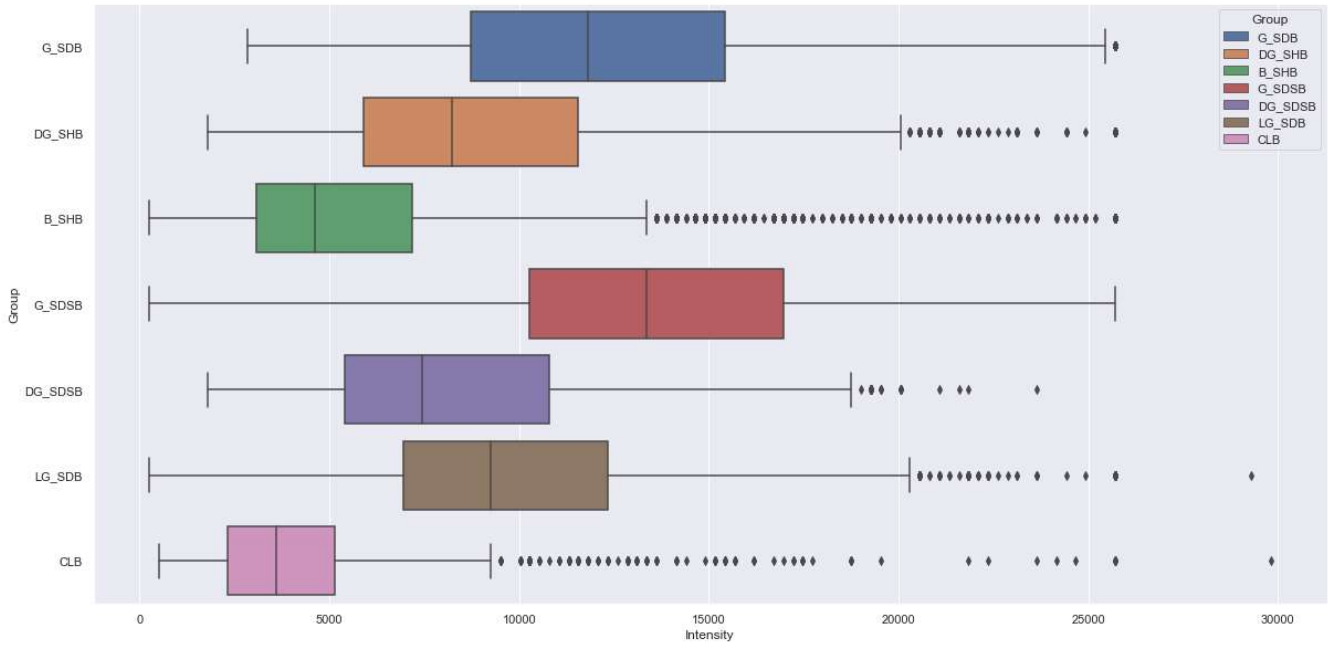

***Figure 4.8**. Boxplot visualization of the point database when distance between LiDAR and sample was 125 cm.*

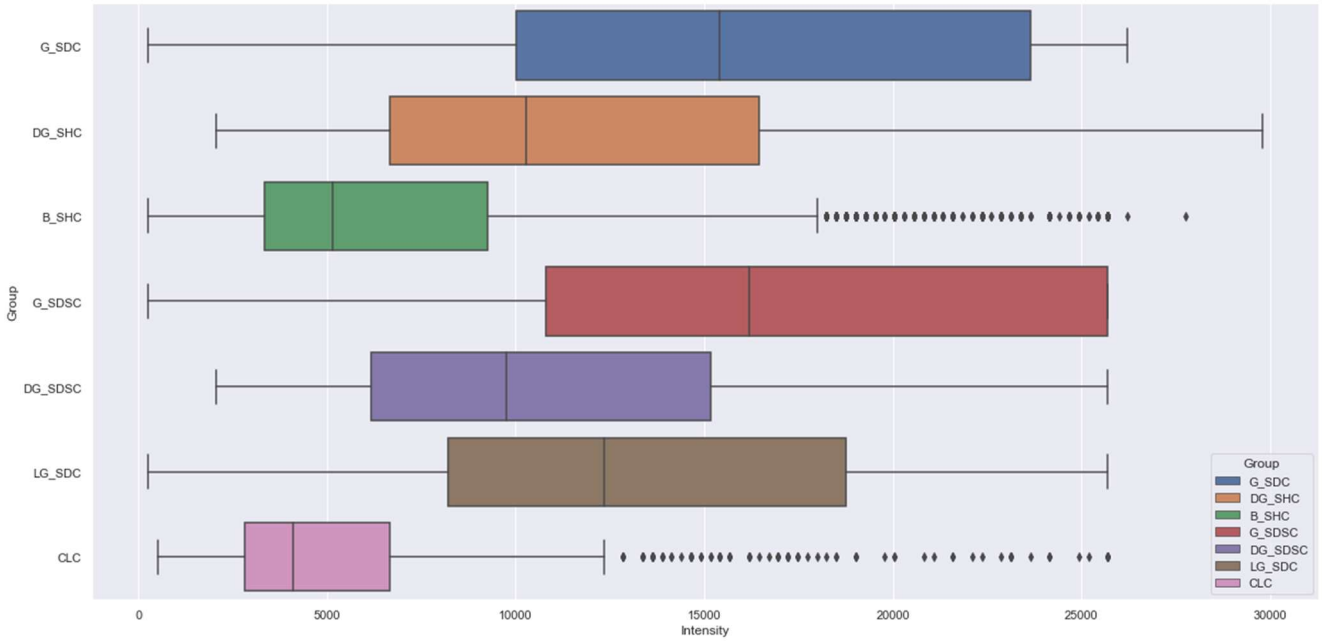

***Figure 4.9**. Boxplot visualization of the point database when distance between LiDAR and sample was 150 cm.*

The One-Way ANOVA (analysis of variance) is the statistical test used to compare the means of three or more different groups, and we applied this statistical method to test if we can use the intensity values to identify different lithologies from the point cloud data. In order to apply ANOVA, data must satisfy the

following assumptions: (i) each group is independent from the other groups, (ii) each group is normally distributed, and (iii) all the groups have equal or similar variances.

The data used in this research meets the first assumption since the data generated from LiDAR measurements were obtained from different rock samples with different lithologies. Therefore, it is easy to conclude that data of the lithology groups used in this research are independent from each other.

The second assumption, each group is normally distributed, was evaluated using the Quantile-Quantile Plot, more commonly known as Q-Q plot or probability plot. It plots the observed values against expected standard normal distribution values. Figures 4.10 to 4.16 show the Q-Q plots of the lithology and distance groups in the database. In these plots, horizontal axis is the expected values according to normal distribution and vertical axis is the measured values. The red line is the best fit line, and ideally we would like to see all the blue data points to be on this line with R^2=1.0 that represents perfect normal distribution of the data. R^2 measures how well the measured data normal distribution. Table 4.4 summarizes the R^2 values according to each lithology and distance category.

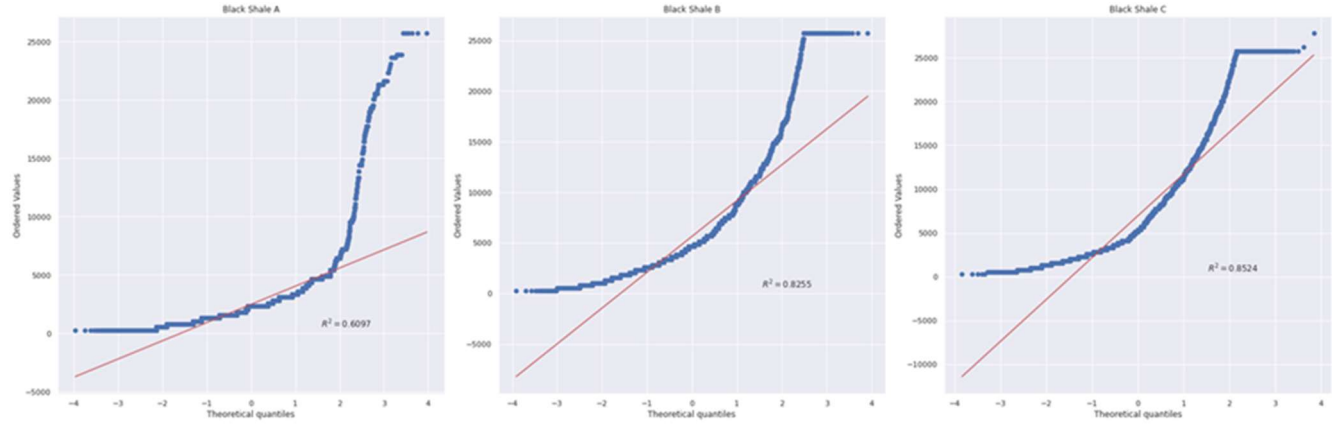

Figure 4.10. *Q-Q plots of Black Shale, distance between sample and LiDAR: 100 cm, 125 cm and 150 cm.*

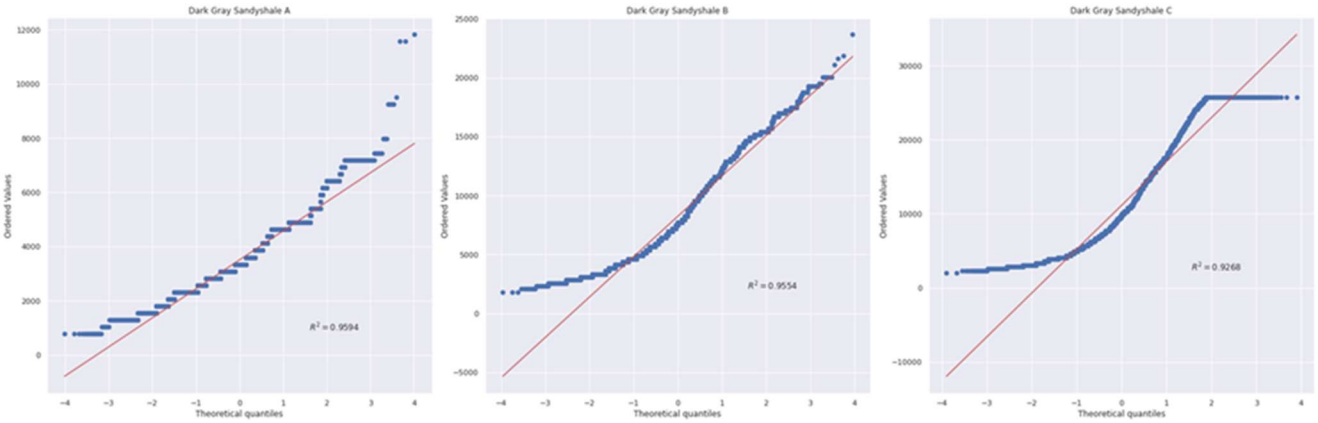

Figure 4.11. *Q-Q plots of Dark Gray SandyShale, distance between sample and LiDAR: 100 cm, 125 cm and 150 cm.*

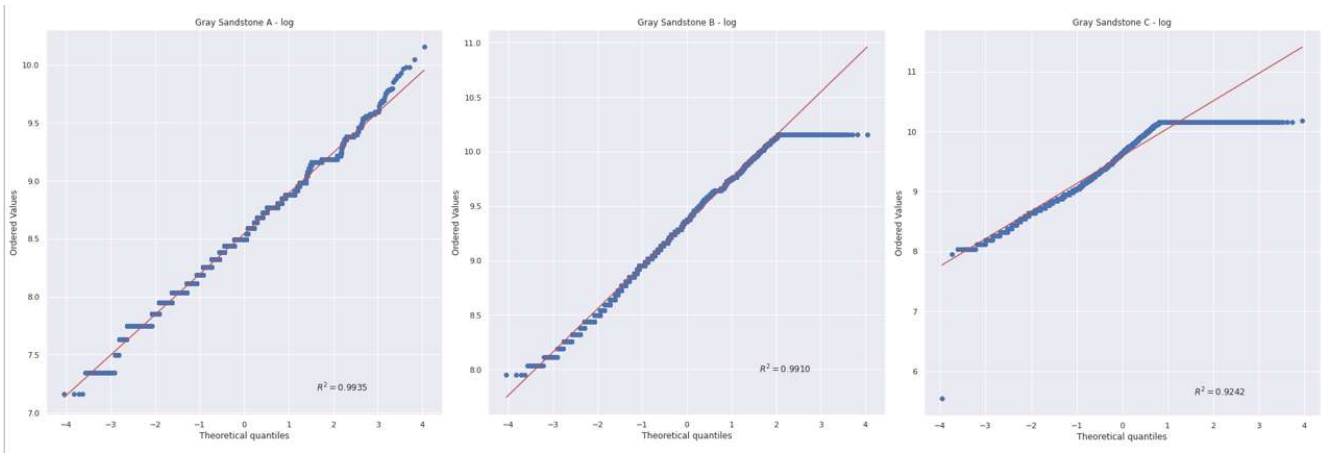

Figure 4.12. *Q-Q plots of Dark Gray Shale, distance between sample and LiDAR: 100 cm, 125 cm and 150 cm.*

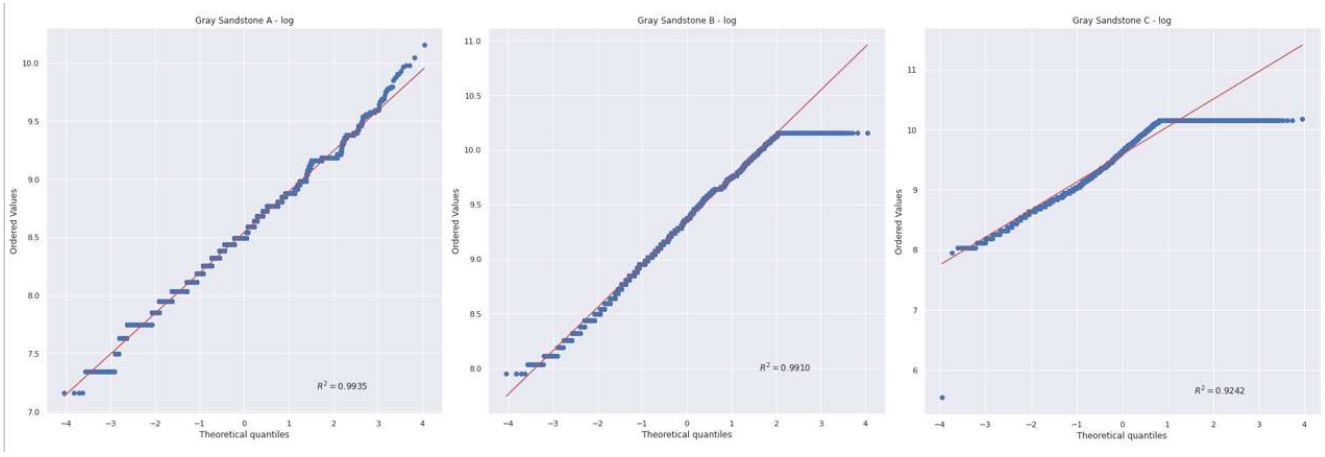

Figure 4.13. *Q-Q plots of Gray Sandstone, distance between sample and LiDAR: 100 cm, 125 cm and 150 cm.*

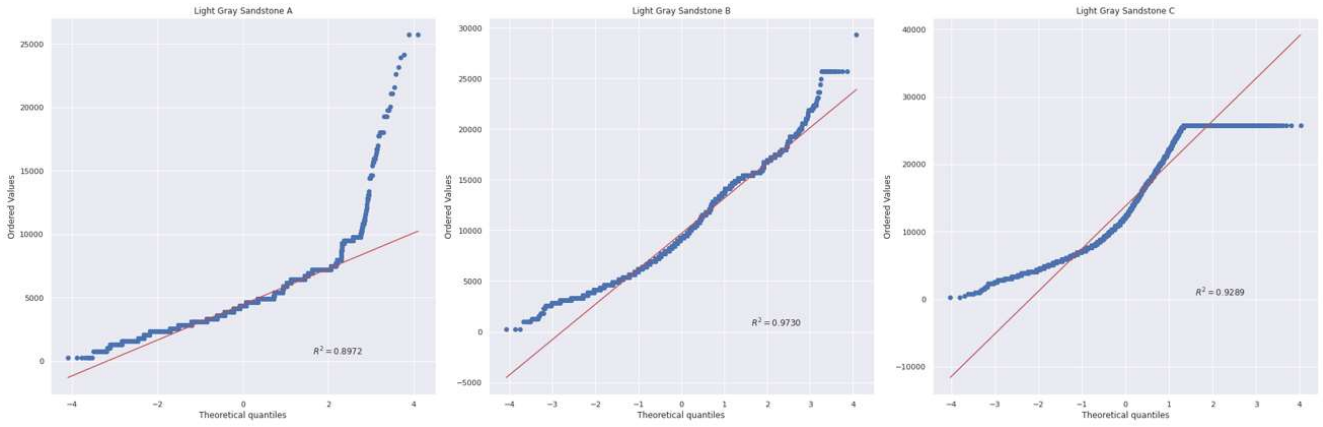

Figure 4.14. *Q-Q plots of Light Gray Sandstone, distance between sample and LiDAR: 100 cm, 125 cm and 150 cm.*

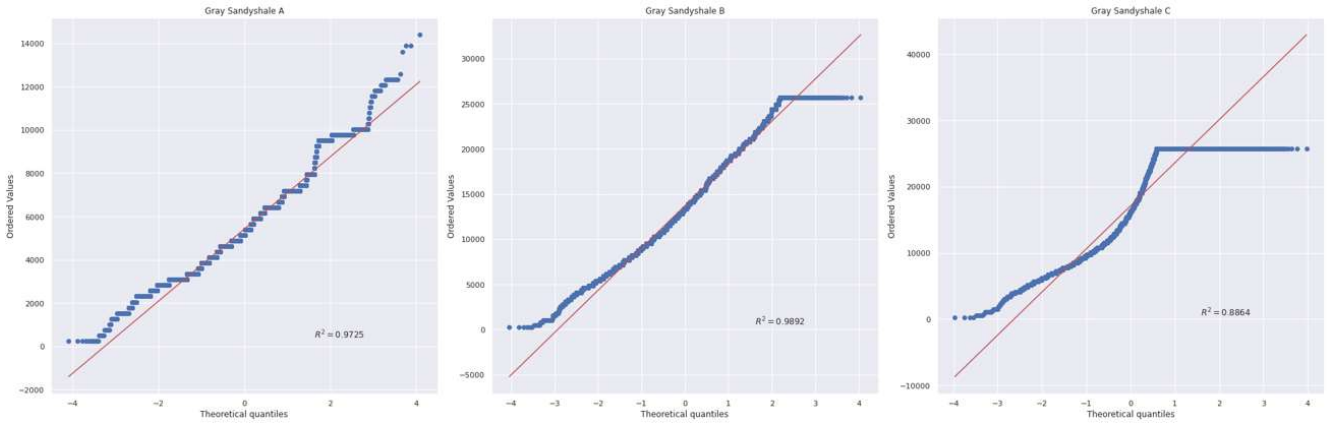

Figure 4.15. *Q-Q plots of Light Gray SandyShale, distance between sample and LiDAR: 100 cm, 125 cm and 150 cm.*

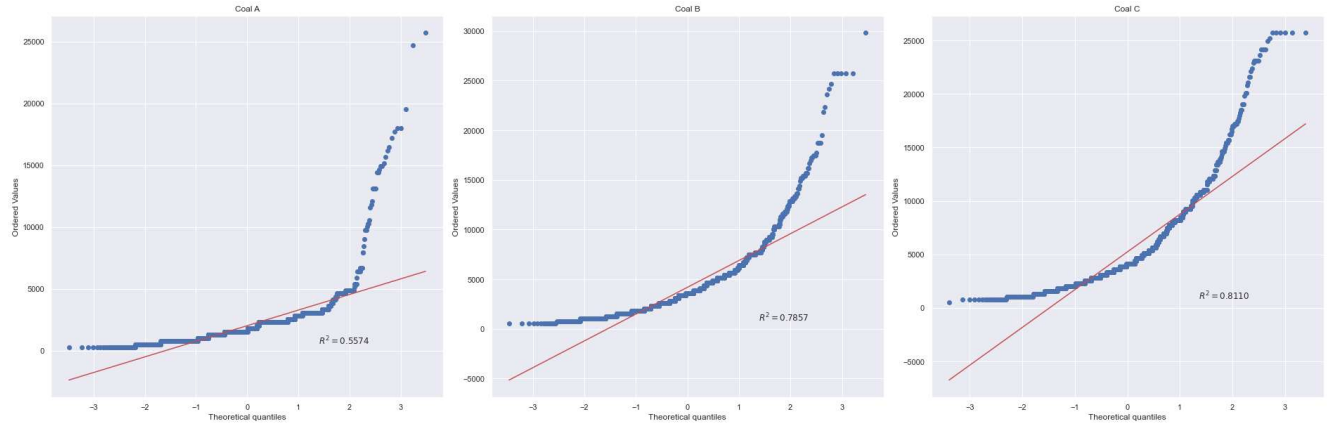

Figure 4.16*. Q-Q plots of Coal, distance between sample and LiDAR: 100 cm, 125 cm and 150 cm.*

Table 4.4. *Summary of the normal fit R^2 values for each lithology and distance category.*

Lithology Group Name	*Distance from the LiDAR*		
	A (100 cm)	*B (125 cm)*	*C (150 cm)*
Black Shale	*0.64*	*0.83*	*0.85*
Dark Gray Shale	*0.90*	*0.96*	*0.92*
Dark Gray SandyShale	*0.96*	*0.96*	*0.93*
Gray SandyShale	*0.97*	*0.99*	*0.89*
Light Gray Sandstone	*0.90*	*0.97*	*0.93*
Gray Sandstone	*0.93*	*0.96*	*0.91*
Coal	*0.56*	*0.79*	*0.81*

R^2 of 0.95 is an acceptable value to conclude that there is a high correlation between the measurement data distribution and normal distribution. When the correlations between the data and normal distribution are low, like for the Black Shale and Coal lithologies in this research, the most common statistical approach is applying transformation to the data to test the normality condition again. The most common transformation function is the natural logarithm. Table 4.5 summarizes the R^2 values after the application

of the logarithmic transformation. Values summarized in Table 4.5 indicates a very strong correlation between transformed measured data and the normal distribution.

Table 4.5. *After logarithmic transformation - summary of the normal fit R^2 values for each lithology and distance category.*

Lithology Group Name	*Distance from the LiDAR*		
	A (100 cm)	*B (125 cm)*	*C (150 cm)*
Black Shale	*0.96*	*0.99*	*0.99*
Dark Gray Shale	*0.97*	*0.99*	*0.97*
Dark Gray SandyShale	*0.98*	*0.98*	*0.98*
Gray SandyShale	*0.97*	*0.95*	*0.89*
Light Gray Sandstone	*0.98*	*0.98*	*0.96*
Gray Sandstone	*0.99*	*0.99*	*0.92*
Coal	*0.95*	*0.99*	*0.96*

The third and final assumption that the data has to satisfy is the homogeneity of variance, also known as homoscedasticity, requiring that different data groups have similar or equal variances. To check this assumption, the variances of all the groups were computed and compared. In each distance group, except Black Shale and Coal, the level of similarity between the variances is considered acceptable. However, since Black Shale and Coal do not satisfying this assumption, application of the standard One-Way ANOVA to this data set is questionable. Instead, we performed Welch's ANOVA test (Welch's F-test) that was designed to test equality of more than two group means when the homogeneity of variance assumption isn't satisfied, although the assumptions of normality and independency are satisfied.

Table 4.6. *After logarithmic transformation - summary of the variances for each lithology and distance category.*

Lithology Group Name	*Distance from the LiDAR*		
	A (100 cm)	*B (125 cm)*	*C (150 cm)*
Black Shale	*0.38*	*0.42*	*0.53*
Dark Gray Shale	*0.13*	*0.21*	*0.34*
Dark Gray SandyShale	*0.10*	*0.19*	*0.34*
Gray SandyShale	*0.11*	*0.15*	*0.22*
Light Gray Sandstone	*0.10*	*0.15*	*0.26*
Gray Sandstone	*0.12*	*0.16*	*0.23*
Coal	*0.36*	*0.42*	*0.46*

Table 4.7 shows the results of Welch's ANOVA test. The null hypothesis for this test is "all different lithology group mean intensities are equal", and the alternative hypothesis is "at least one group mean intensity is different from the others." Results indicated that null hypothesis is rejected (p-value is less than 0.05) and at least one group mean is different from the others. To compare each lithology group, the Games-Howell test is applied. Tables A.1 to A3, in the appendixes, show the pairwise comparison of each lithological group for each distance category. The results indicate that the means of the all the lithology groups are different from each other. Therefore, we can conclude that intensity values can be used to identify different lithological components of the coal rib.

Table 4.7. *After logarithmic transformation – Welch's ANOVA test results for each distance category.*

Distance	Source	Degree of freedom 1	Degree of freedom 2	F	p-value	Np2
A (100 cm)	Lithology	6	30674.754454	11422.30344	0.0	0.389233
B (125 cm)	Lithology	6	27385.713996	9392.56842	0.0	0.34817
C (150 cm)	Lithology	6	21224.562084	5289.702762	0.0	0.275819

Field Experiment:

The third field experiment was conducted to validate that the intensity values can be utilized to estimate the lithology of a coal rib in the field. The coal rib lithology, in the experimental mine, includes rock partings and shale bands and are also partially covered in shotcrete. Point cloud data collected in this experiment was visually analyzed to identify differences the rib lithology.

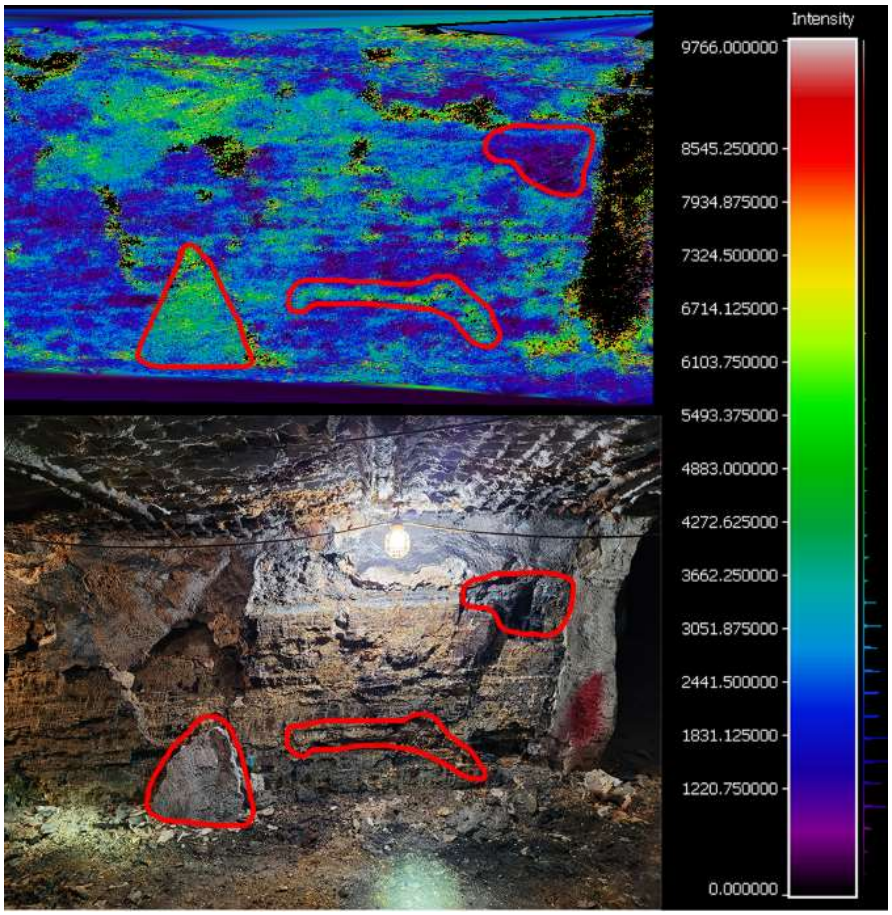

Figure 4.17. *Site 1 photograph and point cloud data, see Figure 3.4.*

Figure 4.17 shows the comparison of the point cloud data collected with the photograph taken at site-1 as shown in Figure 3.4. Portions of the rib covered with shotcrete can be recognized from the point cloud data with the intensity values higher than 5000 (approximately), lower left and middle sections marked on Figure 4.17. Areas where the coal is fully exposed in the upper right corner, intensity values are less than 2000 (approximately).

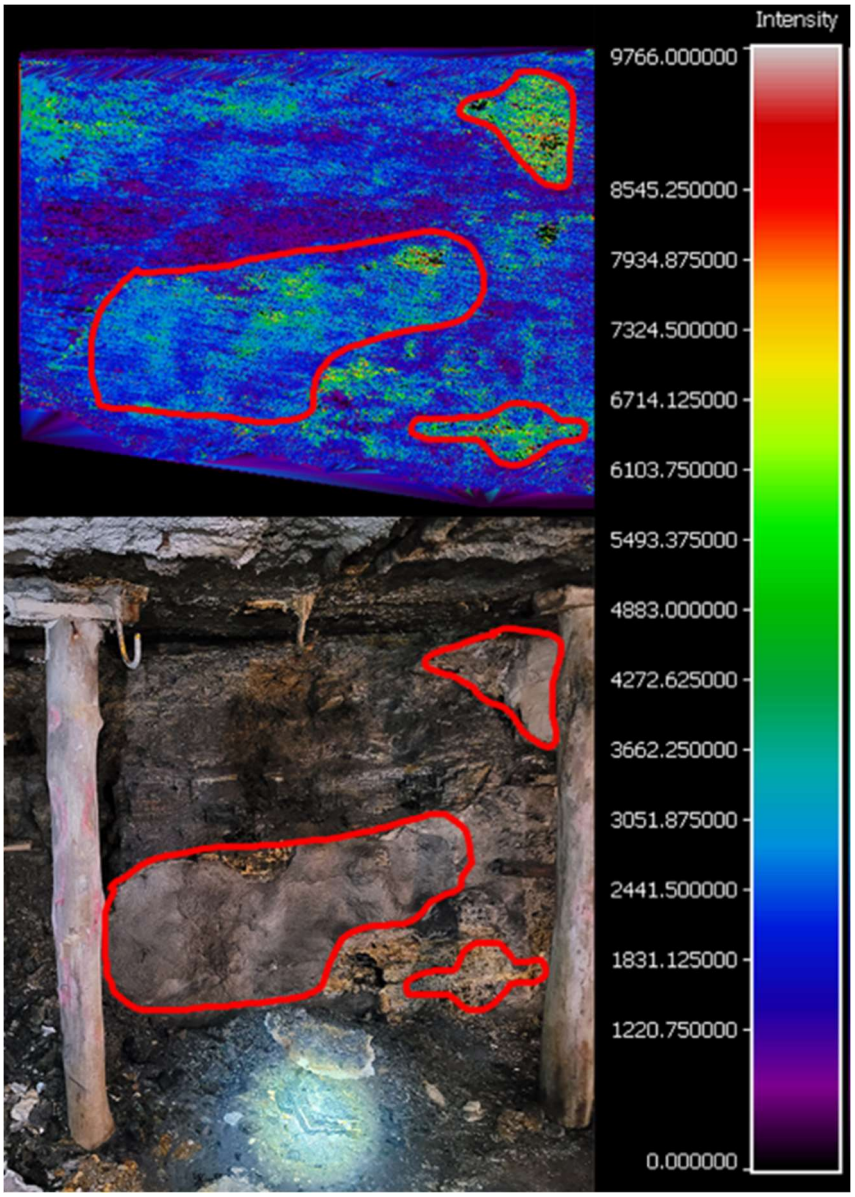

Figure 4.18. *Site 2 photograph and point cloud data, see Figure 3.4.*

Figure 4.18 shows a comparison from site-2. In this figure, partial areas with shotcrete are marked. Again values larger than 5000 can be used to separate shotcrete from the fully exposed coal on the rib. Figure 4.19 from site-3 shows more clearly that the intensity values are less than 2000 represents the coal. In this figure, it is also possible to see the effect of the moisture on the intensity values. Figure 4.20 from site-4 also indicates similar results. Fully exposed coal on the rib can be easily identified from the point cloud data.

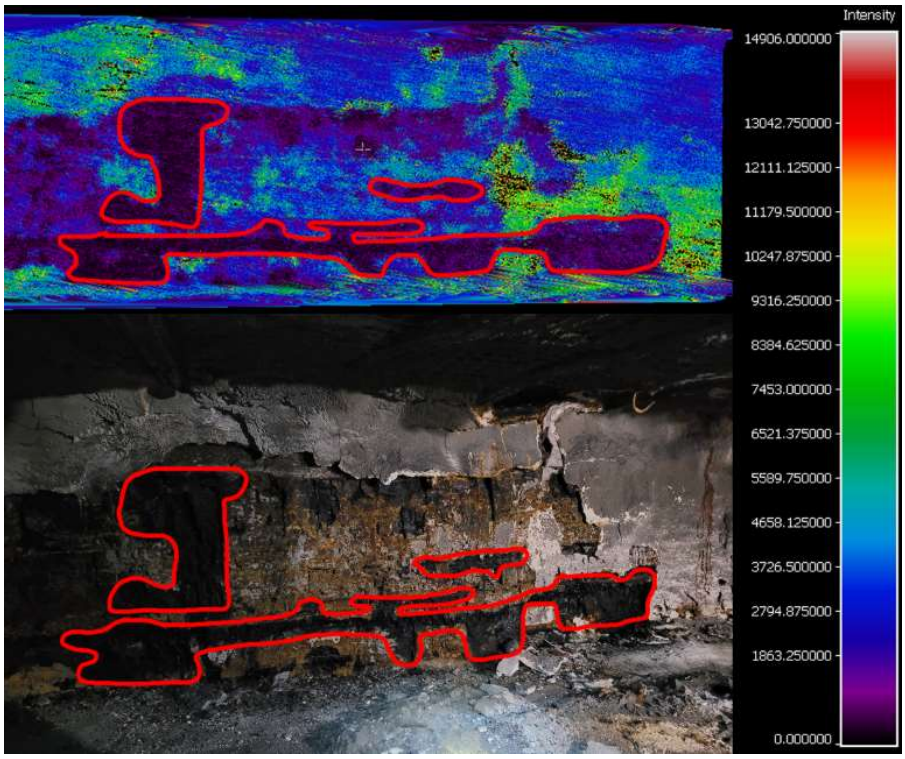

Figure 4.19. *Site 3 photograph and point cloud data, see Figure 3.4.*

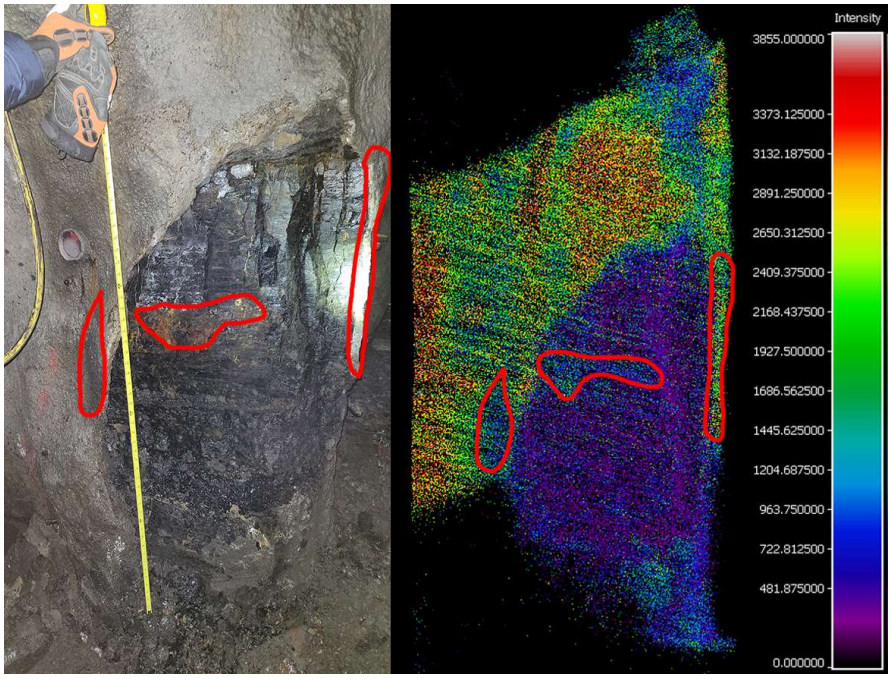

Figure 4.20. *Site 4 photograph and point cloud data, see Figure 3.4.*

5.0 Publication Record and Dissemination Efforts:

1. Gil Hurtado, Francisco Eduardo, "Identification of Rockmass Deformation and Lithological Changes in Underground Mines by Using Slam-Based Lidar Technology" (2023). Graduate Theses, Dissertations, and Problem Reports. 11706. https://researchrepository.wvu.edu/etd/11706

6.0 Conclusions and Impact Assessment:

The research presented here has several results that will help future researchers and survey equipment manufacturers who might work on the adaptation and use of mobile low-cost LIDAR systems with SLAM technology for the underground coal mining sector. Further development of such technology undoubtedly would improve the safety of underground coal mine workers. As part of this research study, (i) a critical review of a LIDAR system that represents the existing technologies was conducted to determine what is necessary to make that system compliant with the requirements for use in a potentially explosive atmosphere. (ii) Data were collected in a controlled laboratory setting and an experimental underground coal mine, and these data were used to evaluate accuracy in the context of rib geology characterization and motion detection.

An overview of the Mine Safety and Health (MSHA) approval process and tests and inspections that might be conducted by MSHA for products such as the GeoSLAM Zeb Horizon portable LiDAR scanner was produced. Potential problem areas were identified with the information at hand; foremost among those are spark-ignition hazards associated with the battery pack and sensor motor. Another significant area of concern identified is the potential lack of motivation of mobile LiDAR manufacturers to expend the resources necessary to redesign the product to meet MSHA's requirements. It was found that the ability of a single entity to fully document and control the design of the product can be problematic, as components such as the sensor and memory sticks are purchased, and the manufacturer may not wish to share the design documentation. It is noteworthy that there are no known issues with the basic technologies used with mobile LiDAR technology. Recommendations were provided for those who wish to design and manufacture a portable LiDAR system for use in gassy underground mines in the United States. This report also provided guidelines and roadmap for developing and getting approval for a permissible mobile LiDAR system.

Additionally, the potential of (i) monitoring rib deformation, movement, or changes and (ii) estimation of coal rib lithology from point cloud data were evaluated. It was found that it is possible to detect changes, as rock falls from ribs or roofs, from mobile LiDAR measurements. In this study, the size of the smallest change that the GeoSLAM Zeb Horizon LiDAR system reliably detected was found to be approximately 6.0 cm. In general, as the number of loops traversed increases, noise in the data decreases and the reliability of the change detection also increases. These results also depend on the algorithms used in this study and the type of LiDAR. Zeb Horizon uses Velodyne VLP-16, 16-channel LiDAR, and a 64-channel LiDAR would be expected to allow detection of the smaller changes. In this research, it was also demonstrated that SLAM-based LiDAR can be used to recognize the changes in the lithology from the mean intensity values. LiDAR measurements of rock cores from various lithologies were first gathered in a lab setting to examine the link between the lithology, the intensity values, and the measurement distance. In-mine tests were then conducted and confirmed the feasibility of using collected LiDAR data to distinguish coal from other lithologies.

7.0 Recommendations for Future Work:

The following research avenues are recommended for future work based on the findings from this research project:

- A critical review of a mobile LIDAR system to determine what is necessary to make that system compliant with the requirements for use in a potentially explosive atmosphere was presented in this report, and potential problem areas were identified. Recommendations were provided for those who wish to design and manufacture a portable LiDAR system for use in gassy underground mines in the United States. This information can be used as a road map to design a LiDAR system and estimate the cost of developing such a system.
- The size of the smallest change that the LiDAR system used in this research reliably detected is concluded as approximately 6.0 cm. Therefore, based on this information, a geotechnical hazard detection method from timelapse LiDAR surveys can be developed for different underground mining sectors.
- A mine-specific lithology estimation method from LiDAR intensity values could be developed, as could a more generalized automated tool with mine-specific parameters.

8.0 References:

Brent A. Slaker, Khaled M. Mohamed, A practical application of photogrammetry to performing rib characterization measurements in an underground coal mine using a DSLR camera, International Journal of Mining Science and Technology, Volume 27, Issue 1, 2017, Pages 83-90, ISSN 2095-2686, https://doi.org/10.1016/j.ijmst.2016.09.032.

CloudCompare. (2016). Introduction - CloudCompare. https://www.cloudcompare.org/doc/wiki/index.php/Introduction

Colwell, M., & Mark, C. 2005. Analysis and Design of Rib Support (ADRS) A Rib Support Design Methodology for Australian Collieries. Retrieved from: Https://stacks.cdc.gov/view/cdc/8506

Dogukan Guner, Samuel Nowak, Taghi Sherizadeh, Maurice Sunkpal, Khaled Mohamed, Yuting Xue, Review of current coal rib control practices, Underground Space, Volume 9, 2023, Pages 53-75, ISSN 2467-9674, https://doi.org/10.1016/j.undsp.2022.04.011.

GEOSLAM. (2020). ZEB-HORIZON User Manual. 1–21.

GeoSLAM. (2021). What is SLAM (Simultaneous Localization and Mapping). https://geoslam.com/us/what-is-slam/

Heasley, K. A., & Chekan, G. (1998). Practical stress modeling for mine planning. In Proceedings of 17th international conference on ground control in mining. July. Morgantown, WV, USA (pp. 129–137).

Heasley, K.A., Nandula, A., & Tulu, I.B. 2018. An Area Calculation of the ARBS Support Intensity. In Proceedings of the 37th International Conference on Ground Control in Mining. Morgantown, WV, pp. 19-23

Karabin, G. J., & Evanto, M. A. (1999). Experience with the boundary-element method of numerical modeling to resolve complex ground control problems. In Proceedings of 2nd International Workshop on Coal Pillar Mechanics and Design. NIOSH IC, USA. (Vol. 9448, pp. 89–114).

Khan, M. U., Zaidi, S. A. A., Ishtiaq, A., Bukhari, S. U. R., Samer, S., & Farman, A. (2021). A Comparative Survey of LiDAR-SLAM and LiDAR based Sensor Technologies. Proceedings of the 2021 Mohammad Ali Jinnah University International Conference on Computing, MAJICC 2021, August. https://doi.org/10.1109/MAJICC53071.2021.9526266

Klemetti, T., Tulu, I.B., & Tuncay, D. 2020. A case study of the stability of a non-typical bleeder entry system at a U.S. longwall mine. International Journal of Mining Science and Technology.

Lawson, H., Zahl, E. & Whyatt, J. (2012). Ground condition mapping: A case study. Preprint number 12-122. In SME Annual Meeting. February 19–22. Seattle, WA, USA.

Lague, Dimitri, Nicolas Brodu, and Jérôme Leroux. "Accurate 3D comparison of complex topography with terrestrial laser scanner: Application to the Rangitikei canyon (NZ)." ISPRS journal of photogrammetry and remote sensing 82 (2013): 10-26.

Mohamed, K. M., Van Dyke, M., Rashed, G., Sears, M.M., & Kimutis, R. 2020. Preliminary Rib Support Requirements for Solid Coal Ribs Using A Coal Pillar Rib Rating (CPRR). In 37th International Conference on Ground Control in Mining.

MSHA, 2019. Accident Injuries Data Set. Retrieved from: https://arlweb.msha.gov/OpenGovernmentData/OGIMSHA.asp

MSHA, 2020. Mine Data Retreival System. Retrieved from https://www.msha.gov/mine-dataretriecal-system

MSHA, 2023a. "Federal Mine Safety & Health Act of 1977, Public Law 91-173, as amended by Public Law 95-164*," MSHA, [Online]. Available: https://arlweb.msha.gov/regs/act/acttc.htm. [Accessed 24 May 2023].

US National Archives, 2023. "eCFR :: 30 CFR Part 18 -- Electric Motor-Driven Mine Equipment and Accessories," US National Archives, 19 March 1968. [Online]. Available: https://www.ecfr.gov/current/title-30/chapter-I/subchapter-B/part-18. [Accessed 24 May 2023].

MSHA,2023b. "Standard Application Procedures For Approval or Evaluation of Intrinsically Safe Apparatus and Associated Apparatus per 30 CFR Part 18, ASAP2016," MSHA, 17 March 2008. [Online]. Available: https://arlweb.msha.gov/techsupp/acc/application/asap2016.pdf. [Accessed 24 May 2023].

UL LLC, 2023a. "UL Standards and Publications, Lithium Batteries, UL 1642," UL LLC, 12 October 2022. [Online]. Available: https://www.shopulstandards.com/ProductDetail.aspx?productId=UL1642. [Accessed 24 May 2023].

MSHA, 2023c. "Standard Application Procedures for Simplified Certification, Certifications and Extensions of Certification, ASAP2015," MSHA, 13 November 2007. [Online]. Available: https://arlweb.msha.gov/techsupp/acc/application/asap2015.pdf. [Accessed 24 May 2023].

MSHA, 2023d. "CRITERIA FOR THE EVALUATION AND TEST OF INTRINSICALLY SAFE APPARATUS AND ASSOCIATED APPARATUS, ACRI2001," MSHA, 04 November 2008. [Online]. Available: https://arlweb.msha.gov/techsupp/acc/application/acri2001.pdf. [Accessed 24 May 2023].

MSHA, 2023e. "Spark Ignition Test, ASTP2232," MSHA, 17 March 2016. [Online]. Available: https://arlweb.msha.gov/TECHSUPP/ACC/StandardTestProcs/ASTP2232.pdf. [Accessed 24 May 2023].

MSHA, 2023f. "Standard Test Procedure – Current Limiting Resistor Adequacy Test, ASTP2206," 09 August 2007. [Online]. Available: https://arlweb.msha.gov/TECHSUPP/ACC/StandardTestProcs/ASTP2206.pdf. [Accessed 24 May 2023].

MSHA, 2023g. "Standard Test Procedure – Maximum Surface Temperature Test, ASTP2233," MSHA, 04 January 2005. [Online]. Available: https://arlweb.msha.gov/TECHSUPP/ACC/StandardTestProcs/ASTP2233.pdf. [Accessed 24 May 2023].

MSHA, 2023h. "Methane Thermal Ignition Test, ASTP2208," 15 October 2015. [Online]. Available: https://arlweb.msha.gov/TECHSUPP/ACC/StandardTestProcs/ASTP2208.pdf. [Accessed 24 May 2023].

MSHA, 2023i. "Battery Flash Current Test, ASTP2202," MSHA, 05 November 2015. [Online]. Available: https://arlweb.msha.gov/TECHSUPP/ACC/StandardTestProcs/ASTP2202.pdf. [Accessed 24 May 2023].

MSHA, 2023j. "Drop Test for Portable Intrinsically Safe Apparatus, ASTP2226," 12 December 2007. [Online]. Available: https://arlweb.msha.gov/TECHSUPP/ACC/StandardTestProcs/ASTP2226.pdf. [Accessed 24 May 2023].

MSHA, 2023k. "Coal Dust Thermal Ignition Test, ASTP2207," 08 April 2016. [Online]. Available: https://arlweb.msha.gov/TECHSUPP/ACC/StandardTestProcs/ASTP2207.pdf. [Accessed 24 May 2023].

MSHA, 2023l. "Force Test of Encapsulated Electrical Assemblies. ASTP2224," 27 October 2015. [Online]. Available: https://arlweb.msha.gov/TECHSUPP/ACC/StandardTestProcs/ASTP2224.pdf. [Accessed 24 May 2023].

MSHA, 2023m. "Piezoelectric Device Impact Test, ASTP2230," 08 April 2016. [Online]. Available: https://arlweb.msha.gov/TECHSUPP/ACC/StandardTestProcs/ASTP2230.pdf. [Accessed 24 May 2023].

MSHA, 2023n. "INTRINSICALLY SAFE ACTIVE VOLTAGE/CURRENT POWER SOURCE CRITERIA, ACRI2011," 20 March 2008. [Online]. Available: https://arlweb.msha.gov/techsupp/acc/application/acri2011.pdf. [Accessed 24 May 2023].

MSHA, 2023o. "Encapsulation Criteria, ACRI2010," 02 July 2009. [Online]. Available: https://arlweb.msha.gov/techsupp/acc/application/acri2010.pdf. [Accessed 24 May 2023].

MSHA, 2023p. "Encapsulation Cable Pull Test, ASTP2241," 16 October 2015. [Online]. Available: https://arlweb.msha.gov/TECHSUPP/ACC/StandardTestProcs/ASTP2241.pdf. [Accessed 24 May 2023].

MSHA, 2023q. "Encapsulation Compound Absorption Test, ASTP2240," 26 October 2015. [Online]. Available: https://arlweb.msha.gov/TECHSUPP/ACC/StandardTestProcs/ASTP2240.pdf. [Accessed 24 May 2023].

MSHA, 2023r. "ENCAPSULATION THERMAL ENDURANCE TEST, ASTP2245," 26 October 2015. [Online]. Available: https://arlweb.msha.gov/TECHSUPP/ACC/StandardTestProcs/ASTP2245.pdf. [Accessed 24 May 2023].

MSHA, 2023s. "Drop Test of Encapsulated Assemblies, ASTP2243," 26 October 2015. [Online]. Available: https://arlweb.msha.gov/TECHSUPP/ACC/StandardTestProcs/ASTP2243.pdf. [Accessed 24 May 2023].

NIOSH, 2023. “Mining Project: Design Methodology for Rib Control in Coal Mines.” Retrieved from: https://www.cdc.gov/niosh/mining/researchprogram/projects/design_methodology.html [Accessed 06 April 2023]

ExRobotics B.V., 2023. "EXR-2," ExRobotics, B.V., [Online]. Available: https://exrobotics.global/robots/exr-2. [Accessed 24 May 2023].

UL LLC, 2023b. "IECEx Certificate of Conformity, IECEx UL 20.0132X," 12 April 2022. [Online]. Available: https://www.iecex-certs.com/#/deliverables/CERT/1508476/view. [Accessed 24 May 2023].

Zofre, 2023a. "Z+F IMAGER® 5006EX," Zoller + Fröhlich GmbH, [Online]. Available: https://www.zofre.de/en/laser-scanners/3d-laser-scanner/z-f-imagerr-5006ex. [Accessed 24 May 2023].

Zofre, 2023b. "IMAGER 5006EX – the world’s only explosion proof 3D laser scanner," [Online]. Available: https://www.mertind.com/argentina/escaneres_industriales/Folleto%20Imager%205006EX.pdf. [Accessed 24 May 2023].

E. C. Magison, Electrical Instruments in Hazardous Locations, Research Triangle Park, NC: Instrument Society of America, 1998.

MSHA,2023t. "Policy Outlining Documentation Requirements for Subassemblies Not Manufactured by the Applicant, APOL2048," 20 April 2016. [Online]. Available: https://arlweb.msha.gov/TECHSUPP/ACC/Approvals/ESD/APOL2048.pdf. [Accessed 24 May 2023].

MSHA, 2023u. "Clarification of Approval Application Evaluation Process," 21 November 2019. [Online]. Available: https://www.msha.gov/sites/default/files/Approval-Applicants-clarification-process.pdf. [Accessed 24 May 2023].

MSHA, 2023v. "UNDERSTANDING AND EXPEDITING THE MSHA INTRINSIC SAFETY APPROVAL PROCESS, Frequently Asked Questions and Guide," 11 June 2015. [Online]. Available: https://arlweb.msha.gov/TECHSUPP/ACC/application/IS_Guide2.pdf. [Accessed 24 May 2023].

Raval, S., Banerjee, B. P., Kumar Singh, S. & Canbulat, I, 2019. A Preliminary Investigation of Mobile Mapping Technology for Underground Mining. In IGARSS 2019 - 2019 IEEE International Geoscience and Remote Sensing Symposium, Yokohama, Japan, pp. 6071-6074.

Rusinkiewicz, Szymon, and Marc Levoy. "Efficient variants of the ICP algorithm." In Proceedings third international conference on 3-D digital imaging and modeling, pp. 145-152. IEEE, 2001.

Optron, 2023. ZEB Horizon. Retrieved from: https://optron.com/geoslam/products/zeb-horizon/ [Accessed 5 May 2023].

Van Dyke, M., Klemetti, T., Tulu, I.B., & Tuncay, D. 2020. Moderate cover bleeder entry and standing support performance in a longwall mine: A case study. In 2020 SME Annual Meeting and Exhibit. Phoenix, AZ: Society for Mining, Metallurgy, & Exploration.

9.0 Appendix:

Table A.1. Pairwise comparison of each lithological group for distance category A – 100cm

Reference Lithology	*Compared Lithology*	*Mean of the Reference Lithology*	*Mean of the Compared Lithology*	*Difference Between Means*	*P-Value*
B_SH	CL	7.616982	7.425176	0.191806	2.54E-14
B_SH	DG_SDS	7.616982	8.112754	-0.495772	3.77E-12
B_SH	DG_SH	7.616982	8.253066	-0.636084	0.00E+00
B_SH	G_SD	7.616982	8.543008	-0.926026	2.11E-11
B_SH	G_SDS	7.616982	8.547907	-0.930925	0.00E+00
B_SH	LG_SD	7.616982	8.352442	-0.73546	1.10E-11
CL	DG_SDS	7.425176	8.112754	-0.687578	0.00E+00
CL	DG_SH	7.425176	8.253066	-0.82789	0.00E+00
CL	G_SD	7.425176	8.543008	-1.117831	0.00E+00
CL	G_SDS	7.425176	8.547907	-1.122731	2.19E-12
CL	LG_SD	7.425176	8.352442	-0.927266	0.00E+00
DG_SDS	DG_SH	8.112754	8.253066	-0.140311	0.00E+00
DG_SDS	G_SD	8.112754	8.543008	-0.430253	0.00E+00
DG_SDS	G_SDS	8.112754	8.547907	-0.435152	0.00E+00
DG_SDS	LG_SD	8.112754	8.352442	-0.239687	0.00E+00
DG_SH	G_SD	8.253066	8.543008	-0.289942	0.00E+00
DG_SH	G_SDS	8.253066	8.547907	-0.294841	0.00E+00
DG_SH	LG_SD	8.253066	8.352442	-0.099376	0.00E+00
G_SD	G_SDS	8.543008	8.547907	-0.004899	5.89E-01
G_SD	LG_SD	8.543008	8.352442	0.190566	0.00E+00
G_SDS	LG_SD	8.547907	8.352442	0.195465	2.65E-11

Table A.2. Pairwise comparison of each lithological group for distance category B – 125 cm

Reference Lithology	*Compared Lithology*	*Mean of the Reference Lithology*	*Mean of the Compared lithology*	*Difference Between Means*	*P-Value*
B_SH	CL	8.43053	8.131192	0.299338	9.83E-13
B_SH	DG_SDS	8.43053	8.920869	-0.49034	0.00E+00
B_SH	DG_SH	8.43053	9.00933	-0.578801	0.00E+00
B_SH	G_SD	8.43053	9.352101	-0.921571	0.00E+00
B_SH	G_SDS	8.43053	9.45954	-1.029011	0.00E+00
B_SH	LG_SD	8.43053	9.108745	-0.678216	6.63E-12
CL	DG_SDS	8.131192	8.920869	-0.789678	0.00E+00
CL	DG_SH	8.131192	9.00933	-0.878139	0.00E+00
CL	G_SD	8.131192	9.352101	-1.220909	9.69E-13
CL	G_SDS	8.131192	9.45954	-1.328348	0.00E+00
CL	LG_SD	8.131192	9.108745	-0.977553	0.00E+00
DG_SDS	DG_SH	8.920869	9.00933	-0.088461	5.61E-12
DG_SDS	G_SD	8.920869	9.352101	-0.431231	0.00E+00
DG_SDS	G_SDS	8.920869	9.45954	-0.538671	7.55E-12
DG_SDS	LG_SD	8.920869	9.108745	-0.187876	0.00E+00
DG_SH	G_SD	9.00933	9.352101	-0.34277	7.25E-11
DG_SH	G_SDS	9.00933	9.45954	-0.45021	1.46E-11
DG_SH	LG_SD	9.00933	9.108745	-0.099415	0.00E+00
G_SD	G_SDS	9.352101	9.45954	-0.10744	0.00E+00
G_SD	LG_SD	9.352101	9.108745	0.243355	0.00E+00
G_SDS	LG_SD	9.45954	9.108745	0.350795	0.00E+00

Table A.2. Pairwise comparison of each lithological group for distance category C – 150 cm

Reference Lithology	*Compared Lithology*	*Mean of the Reference Lithology*	*Mean of the Compared lithology*	*Difference Between Means*	*P-Value*
B_SH	CL	8.590893	8.332324	0.258569	0.00E+00
B_SH	DG_SDS	8.590893	9.156251	-0.565358	0.00E+00
B_SH	DG_SH	8.590893	9.232276	-0.641383	1.81E-11
B_SH	G_SD	8.590893	9.588555	-0.997662	1.71E-12
B_SH	G_SDS	8.590893	9.650573	-1.05968	1.47E-11
B_SH	LG_SD	8.590893	9.408225	-0.817332	0.00E+00
CL	DG_SDS	8.332324	9.156251	-0.823927	2.64E-13
CL	DG_SH	8.332324	9.232276	-0.899952	0.00E+00
CL	G_SD	8.332324	9.588555	-1.256231	0.00E+00
CL	G_SDS	8.332324	9.650573	-1.318249	3.38E-13
CL	LG_SD	8.332324	9.408225	-1.075901	0.00E+00
DG_SDS	DG_SH	9.156251	9.232276	-0.076025	2.92E-11
DG_SDS	G_SD	9.156251	9.588555	-0.432304	1.12E-11
DG_SDS	G_SDS	9.156251	9.650573	-0.494322	0.00E+00
DG_SDS	LG_SD	9.156251	9.408225	-0.251974	0.00E+00
DG_SH	G_SD	9.232276	9.588555	-0.356279	0.00E+00
DG_SH	G_SDS	9.232276	9.650573	-0.418297	8.59E-12
DG_SH	LG_SD	9.232276	9.408225	-0.175949	1.22E-13
G_SD	G_SDS	9.588555	9.650573	-0.062018	2.96E-11
G_SD	LG_SD	9.588555	9.408225	0.18033	6.32E-11
G_SDS	LG_SD	9.650573	9.408225	0.242348	1.35E-11